The Journal of Chemical Physics

RESEARCH ARTICLE | APRIL 25 2024

# Rotational spectrum, structure, and quadrupole coupling of cyclopropylchloromethyldifluorosilane

Alexander R. Davies ; Abanob G. Hanna ; Alma Lutas; Gamil A. Guirgis; G. S. Grubbs, II



*J. Chem. Phys.* 160, 164309 (2024)
https://doi.org/10.1063/5.0203016
CHORUS







AIP Publishing

The Journal of Chemical Physics ARTICLE pubs.aip.org/aip/jcp

# Rotational spectrum, structure, and quadrupole coupling of cyclopropylchloromethyldifluorosilane

Cite as: J. Chem. Phys. 160, 164309 (2024); doi: 10.1063/5.0203016
Submitted: 8 February 2024 • Accepted: 4 April 2024 •
Published Online: 25 April 2024



Alexander R. Davies,[1] Abanob G. Hanna,[2,a)] Alma Lutas,[2] Gamil A. Guirgis,[2] and G. S. Grubbs II[1,b)]

## AFFILIATIONS

[1] Department of Chemistry, Missouri University of Science and Technology, 400 W. 11th St., Rolla, Missouri 65409, USA
[2] Department of Chemistry and Biochemistry, College of Charleston, 66 George St., Charleston, South Carolina 29424, USA

[a)] **Present address:** College of Medicine, University of Florida, 1600 SW Archer Rd., Gainesville, Florida 32610, USA.
[b)] **Author to whom correspondence should be addressed:** grubbsg@mst.edu

## ABSTRACT

Cyclopropylchloromethyldifluorosilane, *c*-$C_3H_5SiF_2CH_2Cl$, has been synthesized, and its rotational spectrum has been recorded by chirped-pulse Fourier transform microwave spectroscopy. The spectral analysis of several isotopologues indicates the presence of two distinct conformations in the free-jet expansion, which are interconvertible through a rotation of the chloromethyl group. A partial substitution structure is presented for the lower energy conformation and is compared to the equilibrium structure obtained from quantum chemical calculations. Additionally, the presence of the chlorine nucleus leads to the rotational transitions splitting into multiple hyperfine components and $\chi_{aa}$, a measure of the electric field gradient along the *a* axis, is unusually small at merely +0.1393(73) MHz. Various common *ab initio* and density functional theory methods fail to predict good quadrupole coupling constants (in the principal axis system) that adequately reproduce the observed hyperfine splitting, although diagonalizing the quadrupole coupling tensor from the principal axis system into a nucleus-centered axis system reveals that, overall, these methods calculate reasonably the electric field gradient about the chlorine nucleus. Finally, a total of nine electric dipole forbidden, quadrupole allowed transitions are observed in the rotational spectra of the parent species of the higher energy conformation and the $^{37}Cl$ isotopologue of the lower energy conformation. These include those of *x*-type (no change in parity of $K_a$ or $K_c$), which, to our knowledge, is the first time such transitions have been observed in a chlorine-containing molecule.





## I. INTRODUCTION

In recent years, we have been investigating the impact on the structure and chemistry of various molecules when one or more carbon atoms are replaced with silicon atoms.[1–8] This paper represents a continuation of our previous work, and herein, we present synthetic details and the results of a detailed rotational study of two distinct conformations (arising from the rotation of the chloromethyl group), and multiple isotopologues, of cyclopropylchloromethyldifluorosilane, *c*-$C_3H_5SiF_2CH_2Cl$.

Microwave studies of substituted cyclopropanes and silanes have been conducted as early as 1962, with Schwendeman and Jacobs recording and analyzing the rotational spectrum of chloromethylsilane[9] and the same group reporting the rotational spectrum of chlorocyclopropane two years later in 1964.[10] Then, in the 1970s, cyclopropylchloromethane was studied by Fujiwara and co-workers[11] and Mohammadi and Brooks,[12] with a more detailed study in 2002 by Heineking *et al.*[13] The latter study was able to resolve the hyperfine splitting, which had not been observed in the two previous investigations. When one considers systems with a silicon atom bound to the cyclopropyl ring, a microwave study exists for cyclopropylfluorosilane,[14] and while we were unable to find any microwave studies for cyclopropyldifluorosilane, cyclopropylchlorosilane, and cyclopropyldichlorosilane, these molecules have been studied by infrared and Raman spectroscopy in Refs. 15–17, respectively. Moreover, more recent microwave studies have investigated molecules that also contain a methyl rotor, such as cyclopropylmethylsilane[18,19] and cyclopropyl(di)fluoromethylsilane,[20] with the latter being, perhaps, the most relevant system studied to the subject of the present

investigation. To our knowledge, no other investigation of any type has been undertaken for the titular molecule: cyclopropylchloromethyldifluorosilane.

Cyclopropylchloromethyldifluorosilane contains a quadrupolar chlorine nucleus (with nuclear spin, $I = 3/2$), which poses the additional challenge of each transition being split into multiple hyperfine components, which complicates the spectrum. As shall be shown, a significant number of transitions arising from this hyperfine splitting are overlapped and unresolved for the lowest energy conformation, even with the resolution that is achieved with our spectrometer. Therefore, it is difficult to determine the nuclear quadrupole coupling constants (NQCCs) to a high degree of certainty, especially $\chi_{aa}$, for that conformation. Nonetheless, from the determined NQCCs, it was possible to achieve a very good understanding of the quadrupole coupling tensor and the differences between different various isotopologues and conformations.

## II. EXPERIMENTAL AND THEORETICAL METHODS

### A. Synthesis

The synthesis of cyclopropylchloromethyldifluorosilane was carried out at the College of Charleston and prepared in two steps, as shown in Fig. 1. Cyclopropylbromide was reacted with magnesium in dry ether using the Grignard method and then coupled with chloromethyltrichlorosilane in dry ether under dry nitrogen gas. The resultant product, cyclopropylchloromethyldichlorosilane, was separated from the ether under reduced pressure and then fluorinated with freshly sublimed antimony trifluoride without solvent. The product was then purified by trap-to-trap distillation several times at reduced pressure and low temperature to isolate pure material at −50 °C. The isolated products were then verified by NMR spectroscopy. $^{1}$H (400 MHz, $CDCl_3$): δ (ppm) −0.06 (m), 1H, CH, 0.70 (m), 2H, $CH_2$, 0.84 (m), 2H, $CH_2$, 2.93 (t), 2H, $CH_2Cl$; $^{13}$C NMR (400 MHz, $CDCl_3$): δ (ppm) 1.52 (s), 23.47 (t); $^{19}$F NMR (400 MHz, $CDCl_3$): δ (ppm) −145.83 (p); $^{29}$Si NMR (400 MHz, $CDCl_3$): δ (ppm) −17.07 (t). The NMR spectra are presented as part of the supplementary material.

### B. Microwave spectroscopy

The microwave spectrum was recorded at the Missouri University of Science and Technology, using our chirped-pulse Fourier transform microwave (CP-FTMW) spectrometer that is described elsewhere,[21,22] in the traditional CP-FTMW configuration. The vapor above the highly volatile, liquid sample at room temperature was seeded in 3 bars Ar and passed through the orifice (~750 μm diameter) of a custom-made sample reservoir,[23] attached to the exterior of a Parker-Hannifin™ Series 9 solenoid valve (620 μs opening time, 3 Hz repetition rate), to form a free-jet expansion.

Owing to having only a limited quantity of sample (≲1 ml), the entire spectrum was recorded using a single 4 μs chirped pulse, encoding the entire 5.0–19.0 GHz region of the electromagnetic spectrum. Three free-induction decays (FIDs) were collected per gas pulse, and ~78 500 FIDs, each 20 μs long, were recorded and averaged together. The averaged FIDs were then fast Fourier transformed into the frequency domain using Kisiel's FFTS[24] software.

Fits for both conformations of cyclopropylchloromethyldifluorosilane observed in the free-jet expansion (and the corresponding minor isotopologues, observed in their natural abundances) were conducted using Pickett's SPCAT/SPFIT[25] package, utilizing Kisiel's AABS[26] user interface, to a Watson S-reduced Hamiltonian in the $I^r$ representation. Western's PGOPHER[27] program was used for the initial fits. Complete lists of transitions, and technical details of the fits, are made available in the supplementary material.

Typically, with this spectrometer, linewidths between ~60–80 kHz at full width at half maximum (FWHM) are expected, and an uncertainty of 10 kHz is attributed to the line centers. While this is true and appropriate for the higher energy conformation, for the lower energy conformation (and therefore the most abundant in the free-jet expansion), the observed transitions were significantly broadened owing to the unresolved hyperfine splitting. Numerous lines were observed with widths exceeding 100 kHz FWHM and, indeed, some greater than 140 kHz FWHM. Consequently, for all isotopologues of the lower energy conformation, we chose to increase the uncertainty to 15 kHz. In the fits, a number of hyperfine transitions are assigned to a single line. Although it is often a matter of judgment as to when this is necessary, these criteria were largely followed: the linewidth was greater than ~80 kHz, all components were predicted to lie underneath the observed line, and there was no significant asymmetry in the lines. This was unnecessary for the higher energy conformation, where the majority of the hyperfine structure was well-resolved. As such, the uncertainty

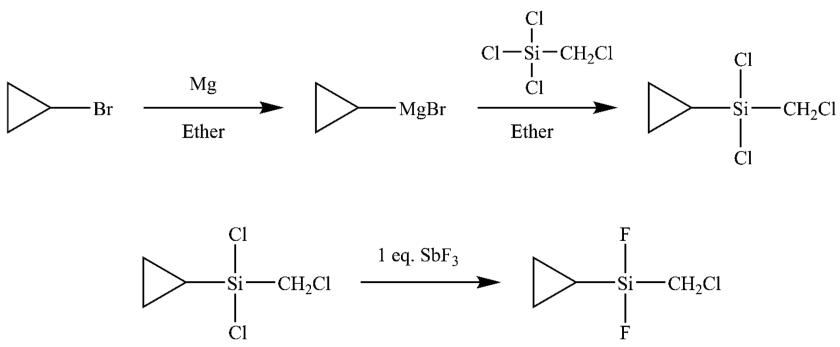


**FIG. 1.** Reaction scheme depicting the synthesis of cyclopropylchloromethyldifluorosilane—see Sec. II A and the supplementary material for full details and NMR data.

that is typically expected with this spectrometer (10 kHz) was retained—although it was still appropriate to assign a handful of the hyperfine transitions to the same line. At the start of the fitting procedure, the well-resolved hyperfine structure was treated before considering the unresolved structure.

### C. Quantum chemical calculations

As is routine in many contemporary spectroscopic studies, the geometry of this molecule has been optimized using various quantum chemical methods, including both *ab initio* and density functional theory (DFT) methods. The augmented triple-ζ basis set, aug-cc-pVTZ, was used for all atoms in all calculations. The expectation from this was to predict geometries and rotational constants that are accurate enough to allow the rotational spectra of the various isotopologues and conformations to be separated and deconvoluted somewhat easily. Additionally, the presence of the quadrupolar chlorine nucleus within the molecule will lead to the transitions being split into multiple hyperfine components and thus a good prediction of the electric field gradient at the chlorine nucleus, and therefore the NQCCs, is essential to understanding rotational spectra where hyperfine splitting is anticipated owing to the additional nuclear spin angular momentum.

The majority of the quantum chemical calculations were performed using the Gaussian 16[28] (Revision C.01) package of computational quantum chemistry programs using the default convergence criteria. The geometries were verified as maxima/saddle points or minima on the potential energy surface by calculating the harmonic vibrational frequencies and checking for the presence or absence of, respectively, any imaginary frequencies. The exception to this was for the QCISD optimization for the lower energy conformation as this was deemed too computationally expensive, although, given the calculated rotational constants and geometric parameter values are in good agreement with those calculated by other methods and the experiment (see also Secs. III C and III F), we are satisfied that the optimized structure corresponds to a minimum on the potential energy surface.

In addition, a rigid potential energy curve for the rotation of the chloromethyl group was also calculated using the Molpro 2021.2[29] package of quantum chemical programs. To do this, the structure of the lowest energy conformation of cyclopropylchloromethyldifluorosilane was reoptimized at the MP2/aug-cc-pVTZ level in Molpro, setting the optimization convergence criteria to be the same as those implemented in Gaussian 16. A "do loop" was used to rotate the Cl–$C_4$–Si–$C_3$ dihedral angle (Fig. 2) in 5° steps, increasing the resolution to a 1° step size around the anticipated locations of the minima and maxima. All geometric parameters were fixed to those of the optimized geometry of the lowest energy conformation, and the z-matrix was set up in such a way that it was possible to fix the

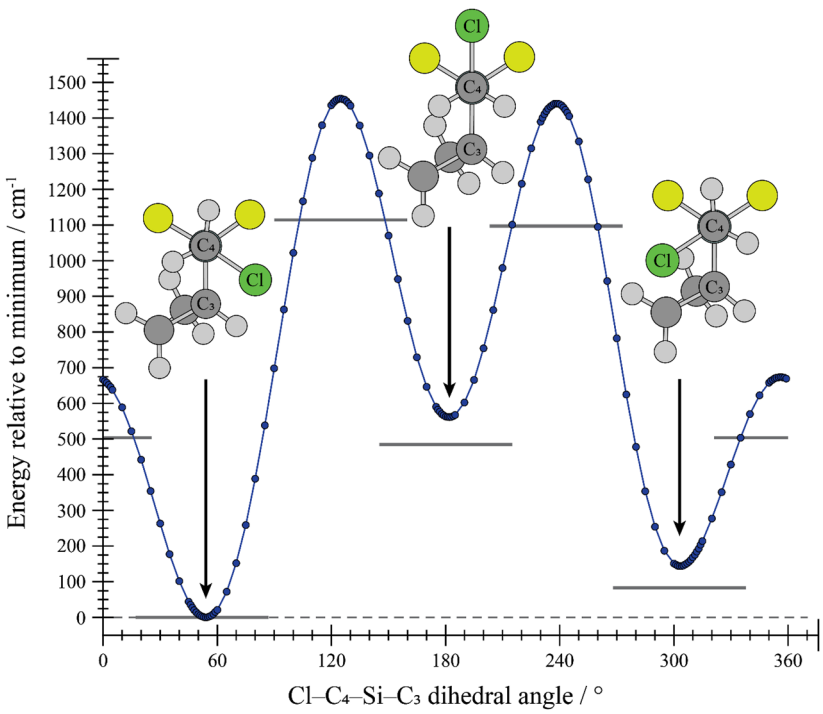


**FIG. 2.** A rigid potential energy curve (calculated using the MP2 method with the aug-cc-pVTZ basis set), arising from rotating the Cl–$C_4$–Si–$C_3$ dihedral angle anticlockwise through a full 360°. Schematics of conformers A, C, and B are given (from left to right) to indicate the approximate geometry of the chloromethyl group (with respect to the rest of the molecule, while viewing down the $C_4$–Si bond) at each minimum. As this is a rigid potential energy scan, the maxima and minima are comparatively higher in energy than those of the optimized geometries—the gray lines represent the energy of the closest, fully optimized stationary point at the MP2/aug-cc-pVTZ level. See Sec. II C for full computational details, and numerical data on the energies and Cl–$C_4$–Si–$C_3$ dihedral angles are tabulated in Table I. The fluorine atoms are colored in yellow, the chlorine atom is in green, the carbon atoms are in gray, the silicon atom is in teal (behind $C_4$), and the hydrogen atoms are in off-white. Only the pertinent atom labels are given.

H–$C_4$–Si–$C_3$ dihedral angles (Fig. 2), which are dependent on the scanned Cl–$C_4$–Si–$C_3$ dihedral angle, to retain the overall geometry of the chloromethyl group while being scanned.

## III. RESULTS AND DISCUSSION

### A. Calculated conformations and geometries

The geometries at the maxima and minima of the potential energy surface, arising from a full 360° rotation of the chloromethyl group, were optimized using both the CAM-B3LYP density functional and the *ab initio* MP2 method. The relative stabilities of the optimized conformations, and the optimized barriers to interconversion, are given in Table I. Both methods predict the conformation with the Cl–$C_4$–Si–$C_3$ dihedral angle of ~55° to be the lowest in energy and henceforth is referred to as conformer A. Conformer A is depicted in the form of a schematic, viewing along the $C_4$–Si bond, on the left of Fig. 2, in which the results of a rigid scan of the Cl–$C_4$–Si–$C_3$ dihedral angle are also presented. Conformer A is also shown in Fig. 3 when viewing the planes defined by the principal axes, as calculated using MP2/aug-cc-pVTZ. Notably, in this conformation, the chlorine atom is *gauche* to one of the fluorine atoms bound to the silicon atom and *anti* with respect to the other. Perhaps most importantly for this conformation, the chlorine atom falls to the opposite side of the $C_4$–Si bond to the cyclopropyl ring (Fig. 2).

The carbon atoms are labeled consistently between all conformations and, therefore, between Figs. 2–4. Notably, the carbon atom at the apex of the cyclopropyl ring, directly bound to the silicon atom, is labeled as $C_3$ and the carbon atom of the chloromethyl moiety is labeled as $C_4$. (The Cl–$C_4$–Si–$C_3$ dihedral angle is defined as 0° when the chlorine atom perfectly eclipses $C_3$, and the dihedral angle increases as the chloromethyl moiety is rotated *anticlockwise* when viewing along the $C_4$–Si bond, with the chloromethyl moiety toward the reader, and can be inferred from Fig. 2.)

Conformer B is obtained from conformer A by rotating the chloromethyl group ~120° *clockwise*, about the $C_4$–Si bond (Fig. 2), past an energy barrier of just over 500 $cm^{-1}$ (Table I), and the equilibrium Cl–$C_4$–Si–$C_3$ dihedral angle is ~305°. Similarly to conformer A, for conformer B, the chlorine atom is also *gauche* to one fluorine atom bound to the adjacent silicon atom and *anti* to the other. This time, the chlorine atom falls to the same side of the $C_4$–Si bond as the cyclopropyl ring and is depicted on the right of Fig. 2 and also in Fig. 4 in the planes as defined by the calculated principal axes. Conformer B is predicted to be the second lowest-energy conformation of cyclopropylchloromethyldifluorosilane between ~83 and 107 $cm^{-1}$ higher in energy than conformer A (when using MP2 and CAM-B3LYP, respectively), and therefore, it is expected to be the second most populous conformation in the free-jet expansion.

It is presumably the mitigation of long-range steric interactions between the chlorine atom and the cyclopropyl ring that makes conformer A lower in energy when compared to conformer B. We do not believe it is interaction with the $-SiF_2-$ unit that is driving the difference in energy between conformers A and B as the relative geometries of both conformations are the same with respect to this (i.e., both have the chlorine atom *gauche* to one fluorine atom and *anti* to the other—see Figs. 2–4).

A third conformation of this molecule, conformer C, was also considered; this has a Cl–$C_4$–Si–$C_3$ dihedral angle of ~180°, where the chlorine atom is pointing directly upward, staggering the two fluorine atoms bound to the nearby silicon atom (see the center of Fig. 2). This conformation is predicted to be about 400 and 484 $cm^{-1}$ higher in energy than conformer A and ~294 and ~401 $cm^{-1}$ higher in energy than conformer B (CAM-B3LYP and MP2, respectively). The difference between the calculated stabilities of conformer C, with respect to conformer B, is significant and arises from the CAM-B3LYP method predicting conformer B to be more unstable and conformer C to be significantly more stable than is predicted by MP2. The spectrum arising from conformer C is not observed, so this conformation is not considered any further.

### B. General remarks on the experimental spectrum

The rotational spectrum of cyclopropylchloromethyldifluorosilane, between 5000 and 19 000 MHz, is presented in Fig. 5. Despite

**TABLE I.** Relative stabilities and barrier heights, with respect to the minimum energy structure, as a function of the Cl–$C_4$–Si–$C_3$ dihedral angle.[a]

| | CAM-B3LYP—optimized[c] | | MP2—optimized[c] | | MP2—rigid[c] | |
|---|---|---|---|---|---|---|
| Nature of stationary point[b] | Dihedral angle (deg) | Energy ($cm^{-1}$) | Dihedral angle (deg) | Energy ($cm^{-1}$) | Dihedral angle (deg) | Energy ($cm^{-1}$) |
| First-order saddle point | −1.73 | 501.32 | −0.99 | 503.47 | −4.00 | 673.60 |
| Minimum (conformer A) | 55.29 | 0.00 | 54.10 | 0.00 | 54.00 | 0.00 |
| First-order saddle point | 124.05 | 958.27 | 124.12 | 1114.29 | 125.00 | 1454.08 |
| Minimum (conformer C) | 180.46 | 400.30 | 181.23 | 484.30 | 182.00 | 561.37 |
| First-order saddle point | 236.65 | 964.63 | 237.20 | 1097.26 | 238.00 | 1440.41 |
| Minimum (conformer B) | 303.71 | 106.55 | 304.97 | 82.92 | 303.00 | 144.04 |

[a]A dihedral angle of zero degrees is defined when the chlorine atom perfectly eclipses $C_3$. The dihedral angle increases as the chloromethyl moiety is rotated *anticlockwise* about the $C_4$–Si bond, when the chloromethyl group is oriented toward the reader—see Fig. 2.
[b]Harmonic frequency calculations verified the nature of the stationary points on the potential energy surface for the optimized structures. The optimized structures pertaining to minima on the potential energy surface all had zero imaginary frequencies, and the structures corresponding to first-order saddle points all had one imaginary frequency. For the rigid potential energy curve, maxima and minima were taken as the lowest and highest local points on the curve, noting the step-size of 1° close to the maxima and minima—see Fig. 2.
[c]The augmented triple-ζ basis set, aug-cc-pVTZ, was used for all atoms in all calculations; see Sec. II C for full computational details.

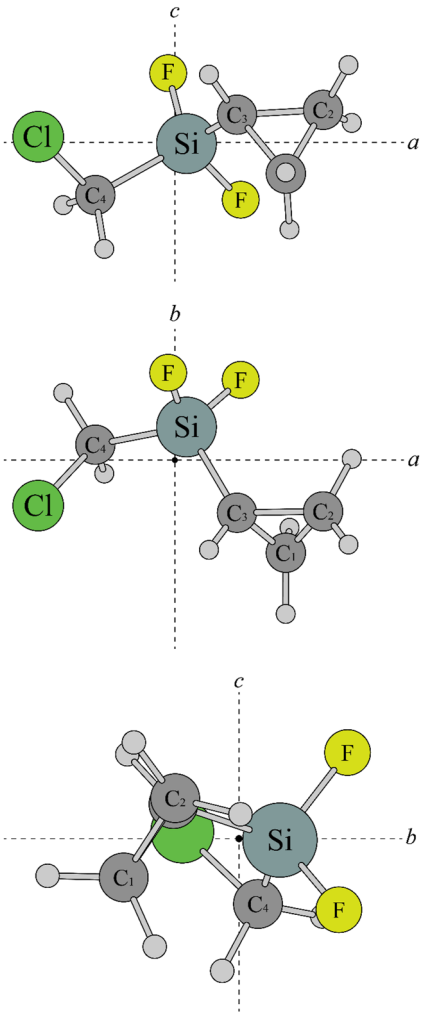


**FIG. 3.** Conformer A in the *ab*-, *ac*-, and *bc*-planes using the structure optimized by the MP2 method and the aug-cc-pVTZ basis set. Carbon, silicon, fluorine, and chlorine atoms are represented by their usual chemical symbols and are color coded as in Fig. 2. The bonds have been drawn in such a way as to offer some perspective into what is pointing in and out of the plane of the paper.

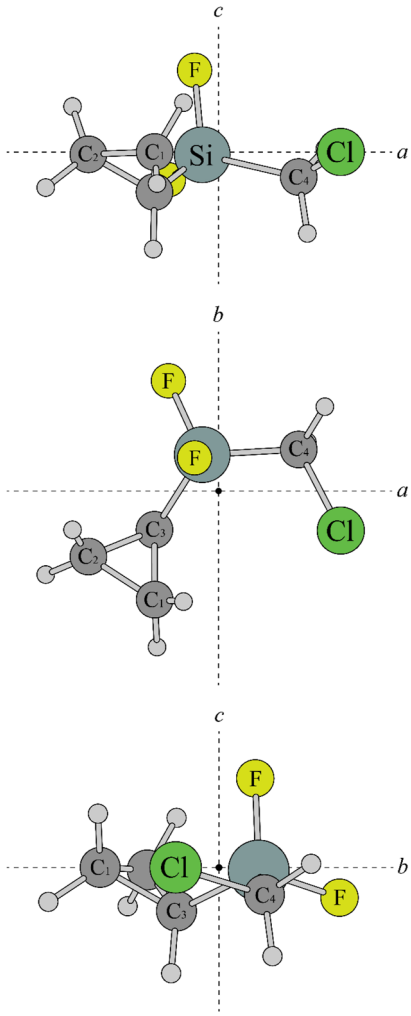


**FIG. 4.** Conformer B in the *ab*-, *ac*-, and *bc*-planes using the structure optimized by the MP2 method and the aug-cc-pVTZ basis set. Carbon, silicon, fluorine, and chlorine atoms are represented by their usual chemical symbols and are color coded as in Fig. 2. The bonds have been drawn in such a way as to offer some perspective into what is pointing in and out of the plane of the paper.

the relatively low number of acquired FIDs, the spectrum is dense, the transitions are spectroscopically bright, and the signal-to-noise ratio is generally good. This allows for the observation of the singly substituted $^{37}$Cl, $^{29}$Si, $^{30}$Si, and (some) $^{13}$C isotopologues, and the $^{37}$Cl–$^{29}$Si and $^{37}$Cl–$^{30}$Si doubly substituted isotopologues, in their natural abundances.

The calculated data for conformer A, as determined by various quantum chemical methods, are presented in Table II. Considering dipole moments, all quantum chemical methods predict $\mu_a < \mu_c < \mu_b$, with $\mu_a$ ~1.0 D, $\mu_c$ ~1.1 D, and $\mu_b$ ~1.4 D. Therefore, one would expect to observe *a*-type transitions with the weakest intensities and *b*-type transitions with the greatest intensities and *c*-type transitions with intensities somewhere in between. This expectation is borne out in the rotational spectrum of the parent species of conformer A where a mixture of *a*-, *b*-, and *c*-type transitions are observed and assigned. This is equally true of the isotopologues of conformer A, where *a*-, *b*-, and *c*-type transitions were observed for all of these. (The parent isotopologue is defined as that which contains the most naturally abundant isotopes for all atoms; in the case of cyclopropylchloromethyldifluorosilane, these are $^{1}$H, $^{12}$C, $^{28}$Si, $^{19}$F, and $^{35}$Cl.) Although there is an issue regarding unresolved hyperfine structure for this conformation, which is discussed further in Sec. III D 1, it can be said that the calculated dipole moments in Table II are largely consistent with the intensities observed in the experimental spectrum (complete lists of the assigned transitions, for all observed isotopologues of both conformers A and B, can be found in the supplementary material).

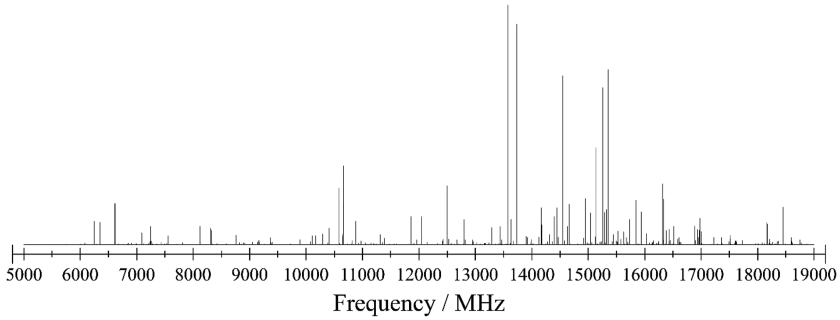


**FIG. 5.** The rotational spectrum of cyclopropylchloromethyldifluorosilane in the 5000–19000 MHz region of the electromagnetic spectrum. The peak at 12 500 MHz is artificial and has had its intensity reduced to show the true molecular signal.

**TABLE II.** Calculated spectroscopic parameters and their values, for conformer A of cyclopropylchloromethyldifluorosilane, using various quantum chemical calculation methods.[a]

| | B3LYP | B3LYP-D3(BJ)[b] | CAM-B3LYP | MP2 | QCISD |
|---|---|---|---|---|---|
| $A_e$ (MHz) | 1927.0712 | 1902.4203 | 1954.9307 | 1919.6825 | 1933.9133 |
| $B_e$ (MHz) | 947.1972 | 974.8578 | 961.0515 | 994.7050 | 977.4399 |
| $C_e$ (MHz) | 797.8195 | 810.9750 | 810.0627 | 826.1294 | 816.7757 |
| $\chi_{aa}$ (MHz) | −2.1809 | −0.4749 | −1.7937 | 0.7192 | −0.3569 |
| $\chi_{bb} - \chi_{cc}$ (MHz) | −8.0646 | −7.6992 | −6.8828 | −3.7614 | −4.5775 |
| $\chi_{ab}$ (MHz) | −39.3180 | −38.7785 | −38.8625 | −36.2302 | 36.6673 |
| $\chi_{ac}$ (MHz) | 34.3488 | 33.9927 | 34.5905 | 33.4530 | 33.5880 |
| $\chi_{bc}$ (MHz) | 35.9424 | 36.6639 | 36.0836 | 36.1189 | −35.5297 |
| $\lvert\boldsymbol{\mu}_a\rvert$ (D) | 1.0515 | 0.9653 | 0.9983 | 0.8967 | 0.9373 |
| $\lvert\boldsymbol{\mu}_b\rvert$ (D) | 1.4387 | 1.4398 | 1.4329 | 1.4120 | 1.3663 |
| $\lvert\boldsymbol{\mu}_c\rvert$ (D) | 1.1563 | 1.1345 | 1.1625 | 1.0980 | 1.1186 |

[a]The augmented triple-ζ basis set, aug-cc-pVTZ, was used for all atoms in all calculations. The NQCCs are calculated using the $^{35}$Cl isotope.
[b]Using Grimme's empirical D3 dispersion[31] with Becke–Johnson damping.[32]

The experimentally determined spectroscopic constants for conformer A are presented in Table III and are discussed in detail in Secs. III C and III D 1. For conformer A, the majority of the transitions observed were R-branch ($\Delta J = +1$) transitions with $\Delta F = +1$. Generally, the individual hyperfine components of these transitions were not distinctly resolvable. This was particularly true for *a*-type transitions, where no transition was fully resolved to show all expected hyperfine components. Additionally, many *b*- and *c*-type transitions were also unresolved; however, a number of these were well split to show all four expected $\Delta F = +1$ hyperfine components—see Sec. III D 1. For the most intense transitions, a handful of $\Delta F = 0$ transitions accompanying the strongest R-branch transitions were observed weakly. In addition, Q-branch ($\Delta J = 0$) transitions were observed in the spectra of the parent species of conformer A and the corresponding $^{37}$Cl, $^{29}$Si, and $^{30}$Si isotopologues and the parent species of conformer B—no P-branch ($\Delta J = -1$) transitions were observed for any isotopologue belonging to any conformation.

At this point, it is worth mentioning that, while we believe we may have observed a number of transitions belonging to the isotopologues arising from $^{13}$C substitution for $C_1$ and $C_2$ (see Fig. 3), too few transitions are observed to obtain a reliable and meaningful fit. Indeed, it was only possible to fit 27 and 30 transitions for the $^{13}C_3$ and $^{13}C_4$ fits, respectively.

In Table IV, both the calculated and experimentally determined values of various spectroscopic parameters are presented for conformer B of cyclopropylchloromethyldifluorosilane. Here, one can see that $\boldsymbol{\mu}_c$ is predicted to be the largest component of the dipole moment by a significant margin. Therefore, one would expect to observe *c*-type transitions as the most intense, with weaker *a*- and *b*-type transitions. Indeed, this was true for the parent isotopologue: the *c*-type transitions were the strongest, and also the most numerous, followed by *b*-type transitions and then *a*-type transitions, in line with the predicted dipole moments. For conformer B, almost all hyperfine transitions were well split, and the majority were R-branch transitions. These were typically resolved into quartets with distinctive intensity patterns, where $\Delta F = +1$; a handful of weak $\Delta F = 0$ transitions were also observed accompanying the strongest $\Delta F = +1$ quartets. As with conformer A, a handful of weak, $\Delta F = 0$, Q-branch transitions were observed. For the $^{37}$Cl isotopologue of conformer B, only R-branch, $\Delta F = +1$, *c*-type transitions were observed; this is likely due to a combination of

**TABLE III.** Experimental spectroscopic parameters, and their values, for all isotopologues observed of conformer A of cyclopropylchloromethyldifluorosilane.[a]

| | Parent | $^{37}$Cl | $^{29}$Si | $^{30}$Si | $^{37}$Cl–$^{29}$Si | $^{37}$Cl–$^{30}$Si | $^{13}C_3$[b] | $^{13}C_4$[b] |
|---|---|---|---|---|---|---|---|---|
| $A_0$ (MHz) | 1948.953 39(16) | 1939.703 71(20) | 1946.479 03(70) | 1944.047 00(84) | 1937.203 5(16) | 1934.732 3(25) | 1940.976 4(29) | 1942.204 3(19) |
| $B_0$ (MHz) | 990.789 740(88) | 968.833 83(12) | 990.721 15(38) | 990.653 22(50) | 968.736 76(82) | 968.642 2(14) | 988.060 1(18) | 985.422 8(11) |
| $C_0$ (MHz) | 826.303 064(91) | 809.406 06(14) | 825.805 95(32) | 825.316 93(32) | 808.898 22(54) | 808.395 27(78) | 823.559 5(10) | 823.596 71(82) |
| $D_J$ (MHz) | $3.061\,5(40) \times 10^{-4}$ | $2.917\,2(67) \times 10^{-4}$ | $3.073(21) \times 10^{-4}$ | $3.094(25) \times 10^{-4}$ | $2.917(34) \times 10^{-4}$ | $3.071(75) \times 10^{-4}$ | $3.098(81) \times 10^{-4}$ | $3.068(75) \times 10^{-4}$ |
| $D_K$ (MHz) | $3.471\,4(23) \times 10^{-3}$ | $3.370\,6(29) \times 10^{-3}$ | $3.482(26) \times 10^{-3}$ | $3.411(38) \times 10^{-3}$ | $3.590(61) \times 10^{-3}$ | $3.676(70) \times 10^{-3}$ | $3.744(78) \times 10^{-3}$ | $3.453(56) \times 10^{-3}$ |
| $D_{JK}$ (MHz) | $-1.280\,0(10) \times 10^{-3}$ | $-1.195\,2(14) \times 10^{-3}$ | $-1.317\,6(87) \times 10^{-3}$ | $-1.308(13) \times 10^{-3}$ | $-1.163(28) \times 10^{-3}$ | $-1.326(43) \times 10^{-3}$ | $-1.481(58) \times 10^{-3}$ | $-1.344(47) \times 10^{-3}$ |
| $d_1$ (MHz) | $-1.211\,5(12) \times 10^{-4}$ | $-1.158\,0(23) \times 10^{-4}$ | $-1.209(12) \times 10^{-4}$ | $-1.223(15) \times 10^{-4}$ | $-1.108(22) \times 10^{-4}$ | $-1.224(43) \times 10^{-4}$ | $-1.161(51) \times 10^{-4}$ | $-1.303(33) \times 10^{-4}$ |
| $d_2$ (MHz) | $-8.666(55) \times 10^{-6}$ | $-8.83(11) \times 10^{-6}$ | $-8.98(73) \times 10^{-6}$ | $-9.30(90) \times 10^{-6}$ | $[-8.83 \times 10^{-6}]$ | $[-8.83 \times 10^{-6}]$ | $[-8.666 \times 10^{-6}]$ | $-1.40(19) \times 10^{-5}$ |
| $\chi_{aa}$ (MHz) | 0.139 3(73) | −0.898 0(93) | [0.139 3] | [0.139 3] | −1.193(93) | −0.99(15) | [0.139 3] | [0.139 3] |
| $\chi_{bb} - \chi_{cc}$ (MHz) | −4.332 0(88) | −2.753(13) | −4.320(35) | −4.204(44) | −2.56(16) | −3.26(29) | [−4.332 0] | [−4.332 0] |
| $\chi_{ab}$ (MHz) | −35.3(17) | −29.96(74) | [−35.3] | [−35.3] | [−29.96] | [−29.96] | [−35.3] | [−35.3] |
| $\chi_{ac}$ (MHz) | 36.9(18) | 28.58(13) | [36.9] | [36.9] | [28.58] | [28.58] | [36.9] | [36.9] |
| $\chi_{bc}$ (MHz) | 37.73(34) | 29.32(43) | 37.8(11) | 37.9(10) | [29.32] | [29.32] | [37.73] | [37.73] |
| $N$[c] | 1217 {870} | 758 {486} | 209 {163} | 164 {124} | 76 {50} | 63 {32} | 27 {27} | 30 {30} |
| MW rms (kHz)[d] | 14 | 13 | 12 | 12 | 10 | 10 | 13 | 10 |

[a]Numbers in brackets give standard errors (67% confidence interval) pertaining to the least significant figures. Numbers in square brackets have been held to the parent value; for the doubly substituted $^{37}$Cl–$^{29}$Si and $^{37}$Cl–$^{30}$Si species, parameter values in square brackets were held to those of the $^{37}$Cl species.

[b]Subscript numbers are index labels for the carbon atoms, as given in Figs. 2 and 3.

[c]Number of transitions included in the fit. This is inclusive of all hyperfine components belonging to each rotational transition. The number of unique frequency lines is given in curly brackets.

[d]MW rms is defined as $\sqrt{\frac{\sum_i (o_i - c_i)^2}{N}}$, where $o_i$ is the observed frequency of the $i$th transition, $c_i$ is its calculated frequency, and $N$ is the number of transitions included in the fit.

**TABLE IV.** Calculated and experimental spectroscopic parameters, and their values, for all isotopologues observed of conformer B of cyclopropylchloromethyldifluorosilane.[a]

| | Calculated[b] | | Experimental | | |
|---|---|---|---|---|---|
| | CAM-B3LYP | MP2 | Parent | $^{37}$Cl (no $\chi_{ac}$)[c] | $^{37}$Cl (with $\chi_{ac}$)[c] |
| $A$[d] (MHz) | 1746.8981 | 1715.0809 | 1738.147 16(23) | 1731.656 61(59) | 1731.656 66(59) |
| $B$[d] (MHz) | 1096.0394 | 1143.1351 | 1137.035 05(18) | 1110.546 33(42) | 1110.546 20(42) |
| $C$[d] (MHz) | 823.7011 | 842.4786 | 842.013 26(14) | 825.914 24(91) | 825.914 11(91) |
| $D_J$ (MHz) | ⋯ | ⋯ | $3.347(14) \times 10^{-4}$ | $2.96(11) \times 10^{-4}$ | $2.95(11) \times 10^{-4}$ |
| $D_K$ (MHz) | ⋯ | ⋯ | $1.415\,5(77) \times 10^{-3}$ | $1.246(53) \times 10^{-3}$ | $1.246(53) \times 10^{-3}$ |
| $D_{JK}$ (MHz) | ⋯ | ⋯ | $-8.083(53) \times 10^{-4}$ | $-6.27(49) \times 10^{-4}$ | $-6.25(49) \times 10^{-4}$ |
| $d_1$ (MHz) | ⋯ | ⋯ | $-1.278\,3(87) \times 10^{-4}$ | $-1.235(49) \times 10^{-4}$ | $-1.233(49) \times 10^{-4}$ |
| $d_2$ (MHz) | ⋯ | ⋯ | $-3.56(29) \times 10^{-6}$ | $[-3.56 \times 10^{-6}]$ | $[-3.56 \times 10^{-6}]$ |
| $\chi_{aa}$ (MHz) | 11.6640 | 13.2217 | 13.925 3(80) | 9.501(21) | 9.502(21) |
| $\chi_{bb} - \chi_{cc}$ (MHz) | −70.7294 | −70.2351 | −73.137(12) | −56.144(17) | −56.144(17) |
| $\chi_{ab}$ (MHz) | −44.0183 | 41.2798 | 43.747(93) | −30.6(10) | 31.1(10) |
| $\chi_{ac}$ (MHz) | −13.4848 | −12.3856 | −13.82(22) | ⋯[c] | [−10.89][c] |
| $\chi_{bc}$ (MHz) | −24.2792 | 23.7485 | 27.50(79) | 20.01(26) | 20.12(26) |
| $N$[e] | ⋯ | ⋯ | 359 {345} | 101 {101} | 101 {101} |
| MW rms[f] (kHz) | ⋯ | ⋯ | 8 | 6 | 6 |
| $\lvert\boldsymbol{\mu}_a\rvert$(D) | 0.5684 | 0.4355 | ⋯ | ⋯ | ⋯ |
| $\lvert\boldsymbol{\mu}_b\rvert$(D) | 0.7166 | 0.6857 | ⋯ | ⋯ | ⋯ |
| $\lvert\boldsymbol{\mu}_c\rvert$(D) | 1.6594 | 1.5998 | ⋯ | ⋯ | ⋯ |

[a]Numbers in brackets give standard errors (67% confidence interval), pertaining to the least significant figures. Numbers in square brackets have been held to the parent value.
[b]The augmented triple-ζ basis set, aug-cc-pVTZ, was used for all atoms in all calculations. The NQCCs are calculated using the $^{35}$Cl isotope.
[c]It was not possible to determine $\chi_{ac}$ for the $^{37}$Cl isotopologue of conformer B. For reasons discussed in the text, two datasets are provided: one where $\chi_{ac}$ is kept out of the quadrupole coupling tensor entirely and one where $\chi_{ac}$, as determined for the parent species, was divided by 1.268 89.[37]
[d]The calculated rotational constants are $A_e$, $B_e$, and $C_e$, and the experimental ones are $A_0$, $B_0$, and $C_0$.
[e]Number of transitions included in the fit. This is inclusive of all hyperfine components belonging to each rotational transition. The number of unique frequency lines is given in curly brackets.
[f]MW rms is defined as $\sqrt{\frac{\sum_i (o_i - c_i)^2}{N}}$, where $o_i$ is the observed frequency of the $i$th transition, $c_i$ is its calculated frequency, and $N$ is the number of transitions included in the fit.



*c*-type transitions being the most intense and also the population of conformer B in the free-jet expansion being too low for the *a*- and *b*-type transitions to have enough intensity to be observed ($^{37}$Cl represents ~24% of naturally abundant chlorine;[30] this conformation is predicted to be a minimum of ~83 cm$^{-1}$ higher in energy than conformer A—see Table I—and it was only possible to acquire 78 500 FIDs).

There is no evidence of internal rotation or large amplitude motion. Unlike the microwave study on cyclopropyldifluoromethylsilane by Dorris *et al.* in Ref. 20, the chloromethyl group in the present investigation leads to multiple stable conformations (at least on the timescale of this experiment) being present in the free-jet expansion, rather than the splitting of transitions due to internal rotation. It is anticipated that the significant mass difference, and therefore moment of inertia, between the methyl and chloromethyl moieties leads to the barrier to complete internal rotation becoming significant in cyclopropylchloromethyldifluorosilane (Table I) and thus unfeasible under jet-cooled conditions. Specifically, Dorris *et al.* determined a $V_3$ potential of 5.2327(26) kJ mol$^{-1}$ (~437 cm$^{-1}$) for the parent isotopologue of the most abundant conformation of cyclopropyldifluoromethylsilane in their free-jet expansion.[20] Conversely, the greatest barrier to interconversion between two conformations of cyclopropylchloromethyldifluorosilane is calculated to be in excess of 950 cm$^{-1}$ (see Table I), and as such, one would not expect to observe complete internal rotation in this molecule, if present, with the resolving power of our spectrometer detailed in Sec. II B. (Notably, in Ref. 20, the authors stated that the majority of the splitting arising from internal rotation was resolved by their CP-FTMW instrument.)

Indeed, some large amplitude motion, e.g., a "flip-flopping" motion between conformers A and B, may be hypothesized as the energetic barrier to interconversion is predicted to be only ~500 cm$^{-1}$—which is comparable to the $V_3$ potential reported in Ref. 20 for cyclopropyldifluoromethylsilane. While there is known partially resolved and unresolved "splitting" for many transitions pertaining to conformer A, which made the rotational spectrum difficult to fit, we prefer to attribute this to the hyperfine structure arising from the unusually small NQCCs in the principal axis system (PAS). This is supported by failing to observe any reciprocal perturbation, or splitting, of the lines in the rotational spectrum of conformer B, where the hyperfine splitting was well resolved, and the linewidths are far narrower—in accordance with expectations for our instrument.

### C. Rotational and centrifugal distortion constants

As presented in Table III, it was possible to determine the rotational constants and all quartic centrifugal distortion constants for multiple minor isotopologues of conformer A. The only exceptions

to this were $^{13}C_3$, where $d_2$ was not determinable and was held to the parent value of $d_2 = -8.666(55) \times 10^{-6}$ MHz and for the $^{37}Cl$–$^{29}Si$ and $^{37}Cl$–$^{30}Si$ doubly substituted species, where the values of $d_2$ were also not determinable but were, instead, held to that determined for the $^{37}Cl$ species—$d_2 = -8.83(11) \times 10^{-6}$ MHz. It was not possible to determine any of the sextic centrifugal distortion constants for any species. The determined rotational constants of each isotopologue are comparable in magnitude to those of the parent isotopologue, reflecting the small changes in mass, and therefore the principal axes, arising from substitution of a single isotope—see also Tables S1(a) and S1(b) of the supplementary material. Additionally, the quartic centrifugal distortion constants for all isotopologues are reassuringly similar to those of the parent—as one might expect. Remarkably different quartic centrifugal distortion constants between isotopologues were interpreted in Ref. 13 as being indicative of misassignments of the transitions and, applying this interpretation here, suggest that misassigned transitions (if any) are not affecting the overall fit to any noticeable degree.

When comparing the experimentally determined rotational constants of the parent species (Table III) to the calculated values (Table II), there is generally good agreement to all levels of theory, both *ab initio* and DFT. The rotational constants for the B3LYP method, without any correction for long-range interactions, are in poorest agreement with the experimental values, which indicates an inadequate optimized structure. It appears that, if using the B3LYP density functional to generate a predicted structure, considering long-range interactions is important (at least for related molecules with this basis set)—whether one uses, for example, the empirical dispersion correction of Grimme and co-workers,[31] DFT-D3 (with, or without, damping functions, such as those of Johnson and Becke,[32] which are utilized herein), or the Coulomb-attenuating method of Yanai, Tew, and Handy.[33] These corrections offer a significant improvement in the agreement with the experimental data with a very small increase in computational cost. Despite these modifications to the B3LYP method performing sufficiently, we emphasize it is the *ab initio* methods in this case that yield the best agreement with the established experimental rotational constants, particularly MP2.

While determining the value of $\chi_{aa}$ was problematic for the parent isotopologue of conformer A (see Sec. III D 1), this did not have an adverse effect on the fits (given the rotational constants are worked out from determining where the transition would be in the absence of any hyperfine splitting). The agreement of the results of the Kraitchman analysis (see Sec. III F) when compared to the structures obtained through quantum chemical calculations appears to confirm this. Despite this, it is accepted that, had it been possible to resolve uniquely all hyperfine components of each rotational transition, the MW rms errors (and also the standard errors attributed to the determined spectroscopic parameter values) associated with these fits would be lower, and it would have been possible to attribute a more typical uncertainty to the line centers. Nonetheless, we are still satisfied that the MW rms errors are indicative of a good fit, which for the parent isotopologue of conformer A is 14 kHz and is the greatest MW rms value of all of the fits—see Table III. However, when judging the MW rms errors here, one needs to consider the elevated attributed uncertainty for this conformation. In addition, there are low uncertainties in the rotational constants and centrifugal distortion constants for the parent isotopologue of conformer A, which, for the latter, all represent less than 0.6% ($d_2$) of the determined values.

In contrast, owing to the hyperfine splitting being very well resolved for conformer B, the MW rms values for the two observed isotopologues of this conformation are notably lower than those for conformer A. For the parent isotopologue of conformer B, the MW rms error is 8 kHz, and for the $^{37}Cl$ isotopologue, the MW rms is 6 kHz (Table IV), which is significantly below the 10 kHz uncertainty attributed to the line centers. These low rms values signify a high-quality fit, to which a high degree of confidence can be placed in the experimentally determined rotational and quadrupole coupling constants. It is acknowledged that the uncertainties of the rotational constants and centrifugal distortion constants are greater than those of conformer A, but this is considered to arise from the significantly smaller number of transitions attributable to this conformation. Indeed, excluding $d_2$ (~8% relative uncertainty), the centrifugal distortion constants for the parent species of conformer B had relative uncertainties of less than 1%, which is not unreasonable, given fewer than ten $J$ levels are observed.

Attributable to the small number of transitions observed for the $^{37}Cl$ isotopologue of conformer B, it was not possible to determine uniquely the quartic centrifugal distortion constant $d_2$, and therefore, this was held to the parent value in the fit, $d_2 = -3.56(29) \times 10^{-6}$ MHz. Finally, very good agreement of the experimentally determined rotational constants of the parent isotopologue of conformer B to both those determined by the CAM-B3LYP density functional and, particularly, the MP2 *ab initio* method is highlighted.

## D. Nuclear quadrupole coupling

### 1. Conformer A

As alluded to in Secs. II B–III C, the hyperfine splitting for conformer A was generally unresolved, with most individual hyperfine components predicted to lie under a single, broad line in the experimental spectrum—this can be seen clearly in Fig. 6(a). This is true for almost all $a$-type transitions and many $b$- and $c$-type transitions; however, a handful of $a$-type transitions split somewhat to yield a partially resolved doublet (and in one case, a partially resolved triplet). This is shown, for example, in insets 3 and 4 of Fig. 6(a). It should be reiterated that no $a$-type transitions for this conformation were resolved fully into the expected quartet of $\Delta F = +1$ components of an R-branch transition in a molecule with a chlorine nucleus. On the other hand, a number of R-branch $b$- and $c$-type transitions were well resolved into these quartets, for example, such a $b$-type transition is shown in inset 2 of Fig. 6(a) and such a $c$-type transition is shown in Fig. 7(a). The dichotomy between some well-resolved and some unresolved $b$-type transitions is apparent in Fig. 6(a), where the very intense but unresolved $8_{0,8}\ F' \leftarrow 7_{1,7}\ F''$ and $8_{1,8}\ F' \leftarrow 7_{0,7}\ F''$ transitions contrast clearly with the nearby and well-resolved $5_{2,3}\ F' \leftarrow 4_{1,4}\ F''$ transition. In addition, an example of a well-resolved $c$-type transition, $6_{1,5}\ F' \leftarrow 5_{0,5}\ F''$, is shown in Fig. 7(a). These transitions (except $5_{2,3}\ F' \leftarrow 4_{1,4}\ F''$) are highlighted as they are common to both spectra of the parent species of conformers A and B, are in a similar energy region, and are intense enough to observe clearly all components of the splitting, if resolvable.

The poorly resolved hyperfine splitting would imply that values of the on-diagonal NQCCs are small, and this expectation is borne out when one considers the experimentally determined on-diagonal

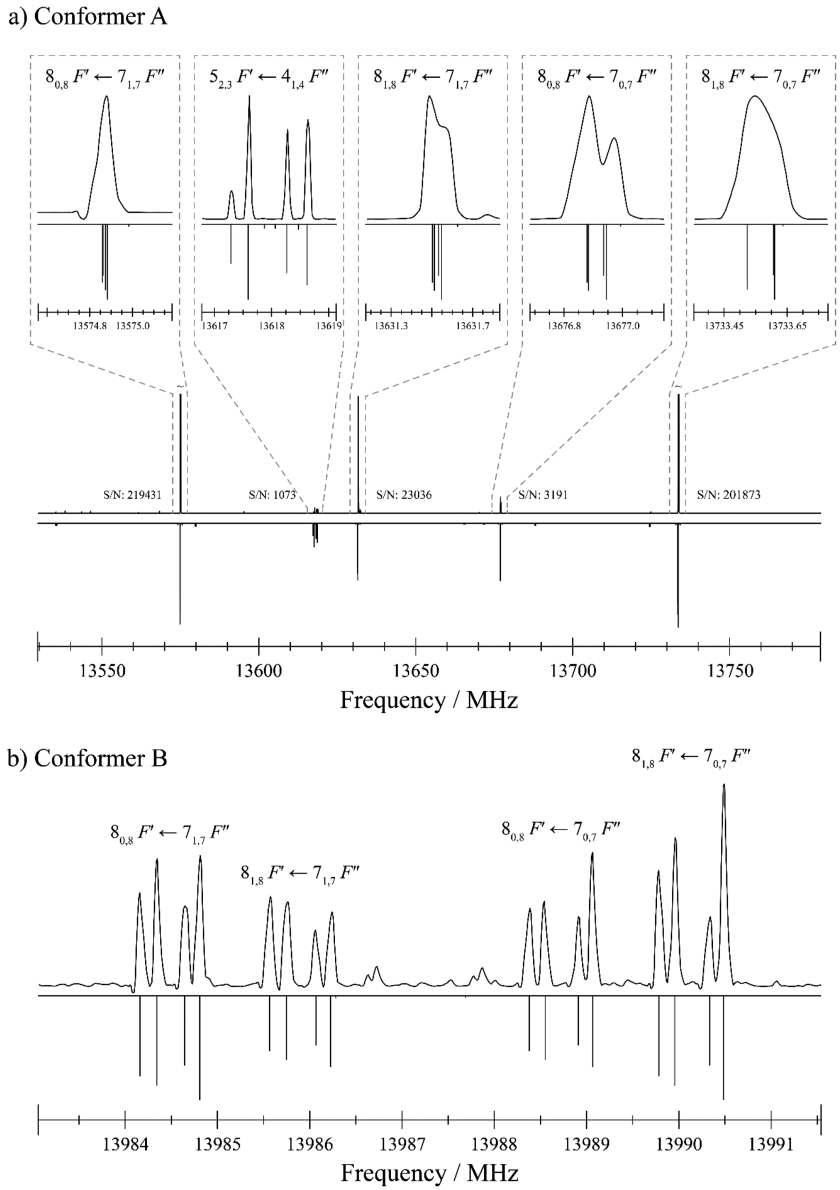


**FIG. 6.** The differences in the typical patterns of the hyperfine splitting for R-branch ($\Delta J = +1$) *a*- and *b*-type transitions in (a) conformer A and (b) conformer B. In both (a) and (b), the experimental spectra are shown upright, and the predicted spectra (from the constants in Tables III and IV for conformers A and B, respectively) are shown inverted. The transitions shown for both conformations have the same quantum numbers (and are given in $J'_{K'_a,K'_c} \leftarrow J''_{K''_a,K''_c}$ notation), except for the $5_{2,3}\ F' \leftarrow 4_{1,4}\ F''$ feature in (a), which is shown to highlight that some *b*-type transitions in conformer A have a well-resolved hyperfine structure (inset 2). Typically, the best resolution of the observed *a*-type transitions in conformer A is a partially resolved doublet, as shown in insets 3 and 4 of (a)—see the text for commentary. In (a), owing to the greater energetic separation of these transitions, zoomed-in views are presented—the abscissa are frequencies in MHz. The unresolved *b*-type transitions in (a) are very intense and have been truncated in the overview spectrum to highlight the less intense transitions, and these have been marked with a tilde ("~"); the intensities of the predicted transitions have not been truncated. Approximate signal-to-noise ratios (*x*:1, where *x* is given here) of the most intense hyperfine component for conformer A (if resolved, otherwise, it is the signal-to-noise ratio of the whole line) are given to provide insight into the relative intensities.

NQCCs presented in Table III: for the parent isotopologue, the value of $\chi_{aa}$ is determined to be +0.1393(73) MHz, and the value of $\chi_{bb} - \chi_{cc}$ is −4.3320(88) MHz. These are unusually small for a chlorine-containing molecule, and notably, the NQCCs in the PAS for a related molecule, 1-chloromethyl-1-fluorosilacyclopentane, are $\chi_{aa}$ = +16.329(21) and $\chi_{bb} - \chi_{cc}$ = −90.528(48) MHz for the $^{35}$Cl isotopologue of the most populous conformation in the free-jet expansion.[6] These represent a value of $\chi_{aa}$ that is nearly 120 times

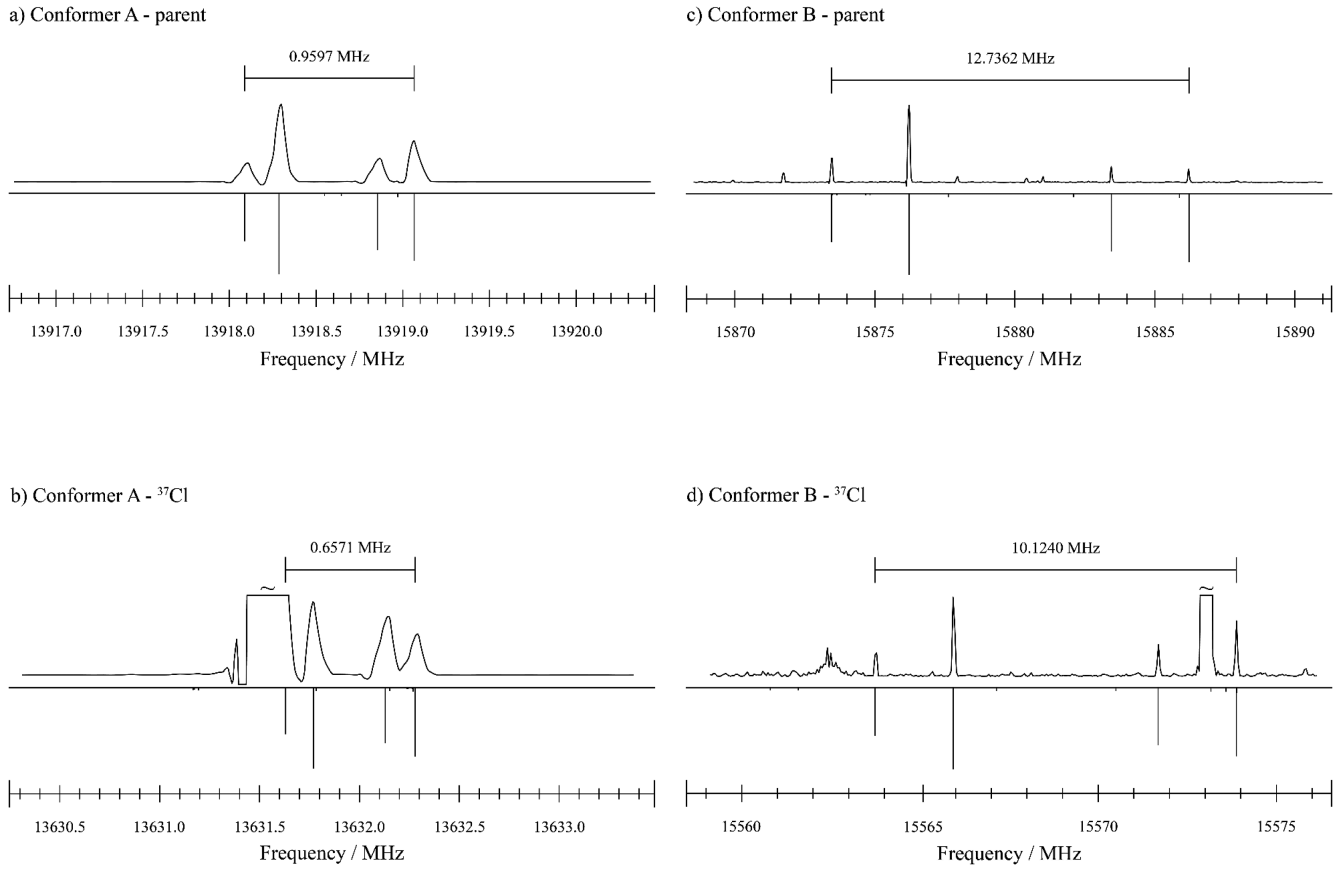


**FIG. 7.** The differences in the patterns of the hyperfine splitting for a well-resolved *c*-type transition ($6_{1,5}$ $F' \leftarrow 5_{0,5}$ $F''$) in (a) the parent species of conformer A, (b) the $^{37}$Cl isotopologue of conformer A, (c) the parent species of conformer B, and (d) the $^{37}$Cl isotopologue of conformer B—the abscissa and ordinate scales are different between the panels, and intense transitions (different from those highlighted here) have been truncated and marked with a tilde ("~"). The differences between the lowest energy *F* transition and highest energy *F* transition are given to provide a sense of scale for the typical splitting patterns of various conformations and isotopologues. Owing to the lowest energy *F* transition in (b) being overlapped by an intense transition arising from the parent species of conformer A, the magnitude of the splitting for this feature is calculated between the experimentally determined transition energy for the higher energy *F* transition and the predicted location of the lower energy *F* transition.

greater and a value of $\chi_{bb} - \chi_{cc}$ that is ~20 times greater, in magnitude than those determined for the parent species of conformer A. However, these constants depend on the location of the quadrupolar nucleus with respect the principal axes, so the NQCCs in the principal axis system are not always directly comparable between molecules. Nonetheless, we retain that these NQCCs in conformer A are unusually small for a chlorine-containing system.

In many cases, a number of hyperfine transitions had to be fit to a single (broad) line. This provides a larger degree of "freedom" for the predicted transitions to shift in frequency underneath the linewidth of the experimentally observed transition(s) without necessarily knowing the correct energy ordering. Therefore, a good estimate of the NQCCs in the PAS was necessary to assign this spectrum successfully. To do this, the geometry of conformer A was optimized using multiple quantum chemical methods to see if a consistent and accurate picture of the NQCCs could be achieved and to see which of the common methods compared best to the experiment. We chose to use the popular density functional, B3LYP, alongside some common augmented versions of it. The more expensive MP2 and QCISD *ab initio* methods are also considered.

Qualitatively, all methods make the same prediction: $\chi_{aa}$ and $\chi_{bb} - \chi_{cc}$ are small, with the former between ~−2.2 and +0.7 MHz and the latter between ~−8.1 and −3.8 MHz (refer to Table II). As concluded in Sec. III C, the standard B3LYP method was less accurate with respect to the rotational constants when not corrected for long-range interactions. This conclusion persists for the NQCCs, which, like the rotational constants, also depend on the locations of the principal axes. Given the already paltry magnitude of the calculated NQCCs, even small differences in these values may lead to radical changes in the predicted hyperfine splitting, such as the energy ordering of the transitions. This was particularly troublesome for conformer A as it was not possible to resolve the majority of the hyperfine transitions in this case.

Surprisingly, only one method considered calculates $\chi_{aa}$ to be positive—and that is MP2—which predicts $\chi_{aa}$ to be +0.7192 MHz and $\chi_{bb} - \chi_{cc}$ to be −3.7614 MHz. Both values are in good agreement

with the experiment, where $\chi_{aa}$ = +0.1393(73) MHz and $\chi_{bb} - \chi_{cc}$ = −4.3320(88) MHz. Moreover, QCISD, which is a more theoretically rigorous method than MP2, predicts $\chi_{aa}$ to be negative, at $\chi_{aa}$ = −0.3569 MHz, in line with the DFT predictions. However, in terms of magnitude, it is in best agreement with the experiment, more so than that predicted by MP2, although the failure to determine the correct sign is a significant flaw with this value. That QCISD calculates $\chi_{aa}$ to be negative could also be an indicator that the ability of MP2 to determine accurately the NQCCs is somewhat fortuitous; however, we maintain that this "accuracy" is useful, nonetheless.

That B3LYP-D3(BJ) predicts a small, negative value of $\chi_{aa}$ (−0.4749 MHz), which is comparable to that predicted by QCISD, is also noteworthy. However, the corresponding prediction of $\chi_{bb} - \chi_{cc}$ is in poorer agreement with the experimental value than that predicted using QCISD—notably, $\chi_{bb} - \chi_{cc}$ is calculated to be −7.6992 MHz by B3LYP-D3(BJ) and −4.5775 MHz by QCISD. The values of $\chi_{bb} - \chi_{cc}$ as calculated by the MP2 and QCISD methods are in good agreement with one another and, in turn, are in reasonable agreement with the experiment, although that calculated by QCISD is closer.

It was also possible to determine experimentally the magnitudes of all three of the off-diagonal NQCCs for the parent species of conformer A and the corresponding $^{37}$Cl isotopologue. While the experiment cannot determine the signs of the individual off-diagonal components of the quadrupole coupling tensor, merely their magnitudes,[34] it is technically possible to determine the sign-product of the three off-diagonal NQCCs by varying it heuristically and noting which has the lower MW rms value. The sign-product of the off-diagonal quadrupole coupling tensor was varied in this manner, and it was not possible to determine whether it was positive or negative to within the uncertainty ascribed to the line centers. Therefore, from the data available, it can be concluded that it is inconsequential whether the overall sign-product is taken to be negative or positive. All theoretical methods considered returned the same overall sign-product (which is negative) although there is, sometimes, disagreement in the signs of the individual off-diagonal NQCCs—for example, MP2 calculates only $\chi_{ab}$ as negative, whereas QCISD predicts only $\chi_{bc}$ as negative. For consistency, in the fits, the signs of the off-diagonal NQCCs were assumed to be those determined by the MP2 method, which was deemed above to be in best agreement, overall, with the experiment. Despite this, it should be highlighted that even were it possible to determine the overall sign-product of the off-diagonal part of the quadrupole coupling tensor, it would not matter (from the perspective of a microwave spectroscopic experiment) whether one selects $\chi_{ab}$, $\chi_{ac}$, $\chi_{bc}$, or all three, to be negative.

Another useful tool to assist with the understanding of the nuclear quadrupole coupling is to diagonalize the quadrupole coupling tensor into a nucleus-centered axis system, whereby the $z$ axis is the steepest gradient and is assumed to occur along (or very close to) the C–Cl bond. Doing this eliminates any differences in the calculated NQCCs owing to differences in the geometry and therefore the locations of the principal axes. This also enables comparisons with isotopologues, conformations, and even different chlorine-containing molecules (Table V), and one can use the diagonalized quadrupole coupling tensor as an indirect probe to establish and understand any changes in the C–Cl bonding environment between systems. A complete quadrupole coupling tensor is required to get the most accurate results from diagonalization in this manner, and here, this method can be used as a tool to check for self-consistency of the determined NQCCs in the PAS between isotopologues if the complete quadrupole coupling tensor of each isotopologue is available. We continue to assume that only $\chi_{ab}$ is negative, based on the reasoning above, although which off-diagonal NQCC is assumed to be negative will not affect the magnitudes or signs of $\chi_{zz}$ and $\eta$ (these are the quadrupole coupling constant along the $z$ axis and the asymmetry parameter), provided that the sign-product of the off-diagonal NQCCs remains the same.

The quadrupole coupling tensor was diagonalized using Kisiel's QDIAG program, available on the PROSPE website.[35] In Table VI, the values of $\chi_{zz}$ and $|\eta|$ for the parent species of conformer A are

**TABLE V.** A comparison of the values of $\chi_{zz}$[a] and $|\eta|$[b] for related molecules.

| | $^{35}$Cl | | $^{37}$Cl | | |
|---|---|---|---|---|---|
| | $\chi_{zz}$ (MHz) | $\lvert\eta\rvert$ | $\chi_{zz}$/MHz | $\lvert\eta\rvert$ | References |
| Conformer A | −73.3(17) | 0.065(30) | −58.61(59) | 0.017(12) | This work |
| Conformer B | −76.09(38) | 0.0264(87) | −55.89(77)[c] | 0.071(15)[c] | This work |
| Chloromethane | −74.7514(11) | ⋯ | −58.9116(34) | ⋯ | 36 |
| Chlorocyclopropane | −71.40(51) | 0.029(11) | ⋯ | ⋯ | 10 |
| Chloromethylcyclopropane | −70.57(12) | 0.0162(67)[d] | −55.50(12) | 0.019(10)[d] | 13 |
| Chloromethylsilane | −68.7(16) | 0.048(16) | ⋯ | ⋯ | 9 |
| Chloromethylfluorosilane | −73.53(70)[d] | 0.0497(95)[d] | −57.51(61)[d] | 0.058(11)[d] | 62 |
| 1-Chloromethyl-1-fluorosilacyclopentane | −70.6(37) | 0.050(53)[d] | −54.76(11)[d] | 0.0610(31)[d] | 6 |
| HCl | −67.618 93(47) | ⋯ | ⋯ | ⋯ | 63 |

[a]It is assumed that the $z$ axis lies along, or very close to, the Cl–C bond.
[b]This is a measure of the asymmetry of the electric field gradient along the $z$ axis, $\eta = \frac{\chi_{xx} - \chi_{yy}}{\chi_{zz}}$. A value of zero indicates perfect cylindrical symmetry.
[c]From the quadrupole coupling tensor including $\chi_{ac}$. See Sec. III D 2 and Table VII for further details.
[d]Value generated from the data presented in the corresponding reference.

**TABLE VI.** Nucleus-centered nuclear quadrupole coupling constants (NQCCs) resulting from the diagonalization of the quadrupole coupling tensor for select isotopologues of conformer A of cyclopropylchloromethyldifluorosilane.

| | Calculated[a] | | | Experimental[b] | | | | | |
|---|---|---|---|---|---|---|---|---|---|
| | CAM-B3LYP | MP2 | QCISD | Parent | $^{37}$Cl | $^{29}$Si | $^{30}$Si | $^{37}$Cl–$^{29}$Si | $^{37}$Cl–$^{30}$Si |
| $\chi_{zz}$[c] (MHz) | −73.2357 | −70.6132 | −70.6153 | −73.3(17) | −58.61(59) | −73.35(74) | −73.42(67) | −58.610(53) | −58.619(91) |
| Ratio[d] | ⋯ | ⋯ | ⋯ | ⋯ | 1.251(32) | 0.999(25) | 0.998(25) | 1.251(29)/1.000(10) | 1.250(29)/1.000(10) |
| $\lvert\eta\rvert$[e] | 0.0188 | 0.0213 | 0.0190 | 0.065(30) | 0.017(12) | 0.0657(94) | 0.0657(88) | 0.0219(16) | 0.0194(27) |

[a]The augmented triple-ζ basis set, aug-cc-pVTZ, was used for all atoms in all calculations. The NQCCs are calculated using the $^{35}$Cl isotope.
[b]The value of $\chi_{zz}$ for chloromethane is −74.7514(11)—see Ref. 36.
[c]It is assumed that the $z$ axis lies along, or very close to, the Cl–C bond.
[d]This is the ratio of the experimentally determined value of $\chi_{zz}$ to that of the parent. For the $^{37}$Cl–$^{29}$Si and $^{37}$Cl–$^{30}$Si doubly substituted species, the corresponding ratios to the $^{37}$Cl isotopologue are also given after the forward slash ("/"). The uncertainty is based on the propagation of the errors in the values of $\chi_{zz}$. The theoretical ratio between the quadrupole moments, $Q$, of atomic chlorine, $Q(^{35}\text{Cl})$ and $Q(^{37}\text{Cl})$ should be ~1.268 89(3)[37,38]—see the text for commentary.
[e]This is a measure of the asymmetry of the electric field gradient along the $z$ axis, $\eta = \frac{\chi_{xx}-\chi_{yy}}{\chi_{zz}}$. A value of zero indicates perfect cylindrical symmetry.

presented alongside the corresponding values for the $^{37}$Cl, $^{29}$Si, and $^{30}$Si isotopologues and those calculated by various theoretical methods. The parameter $|\eta|$ is a measure of the cylindrical symmetry of the electric field gradient about the $z$ axis, and a value of zero represents perfectly cylindrical symmetry. Only the absolute value is meaningful as, once the $z$ axis is defined, the choice of which orthogonal axis is $x$ and which is $y$ is arbitrary, although $\chi_{yy}$ is taken, consistently, to be that with the second largest magnitude, which then yields a positive value of $\eta$. The errors in $\chi_{zz}$ and $|\eta|$ in Table VI are based on the propagation of the standard errors in the NQCCs in the PAS in Table III; where an NQCC was held to the corresponding parent value in the fit, the error on that parameter value was set to zero. The quadrupole coupling tensors of the observed $^{13}$C isotopologues are not considered here as it was not possible to assign enough individual hyperfine transitions to determine any of the NQCCs in the PAS and they had to be held to the values of the parent for the fit—see Table III. For the silicon isotopologues, $\chi_{aa}$, $\chi_{ab}$, and $\chi_{ac}$ were held to the values determined for the parent species, as it was only possible to determine $\chi_{bb} - \chi_{cc}$ and $\chi_{bc}$, and thus the reported errors in $\chi_{zz}$ and $|\eta|$ for these species are notably lower than those for the parent. In addition, only the on-diagonal part of the quadrupole coupling tensor was determinable to a sufficient degree of certainty for the $^{37}$Cl–$^{29}$Si and $^{37}$Cl–$^{30}$Si doubly substituted isotopologues. As the quadrupolar nucleus here is $^{37}$Cl, the off-diagonal NQCCs were held to those determined for the $^{37}$Cl isotopologue. It is acknowledged that this decision, alongside the relatively high uncertainty in the on-diagonal NQCCs, will likely affect the values of $\chi_{zz}$ and $|\eta|$ for these species, but it is maintained that these give comparable and meaningful results (*vide infra*).

By fixing the NQCCs in the PAS in this manner, a fundamental assumption is made: the principal axes do not change significantly upon isotopic substitution. This seems to be a reasonable assumption, particularly for silicon, given that, in Fig. 3, one can see that the silicon atom is very close to the center of mass—see also Tables S2(a) and S2(b) of the supplementary material—hence, one would expect the change in the locations of the principal axes to be minimal, given that the substitution is, at most, an additional 2 $m_u$. This expectation is borne out when one considers the rotational constants in Table III—$A_0$, $B_0$, and $C_0$ for the $^{29}$Si and $^{30}$Si isotopologues are very similar to those of the parent, indicating little change in the principal axes. Additionally, there is a similarly small change in $\chi_{bb} - \chi_{cc}$ and $\chi_{bc}$, although the former may be somewhat "by design" as the quadrupole coupling tensor is traceless, and the value of $\chi_{aa}$ was fixed, meaning that $\chi_{bb} + \chi_{cc}$ must equal $-\chi_{aa}$. Despite there being freedom for $\chi_{bb}$ and $\chi_{cc}$ to vary, the extent of which is restricted by how much the other varies. While this assumption is poorer for isotopic substitution of chlorine in the doubly substituted species as the chlorine atom is further away from the center of mass—see Fig. 3 and Tables S2(a) and S2(b) of the supplementary material—one can see from the MW rms values (Table III) that holding the off-diagonal NQCCs in this manner does not have a detrimental impact on the quality of the fit. This could be because the off-diagonal NQCCs are not required in the Hamiltonian to reproduce adequately the rotational spectra of these species with the number of transitions observed. Moreover, these held off-diagonal NQCCs are also comparable in magnitude to those calculated by MP2/aug-cc-pVTZ—see Table S1(a) of the supplementary material—and it is concluded that the NQCCs in the PAS are adequate when calculated using this

method (*vide supra*). At this point, it is a matter of judgment as to whether one should continue to keep the off-diagonal NQCCs in the Hamiltonian or whether to remove them entirely, but, in this instance, we prefer to retain them in the quadrupole coupling tensor as it is possible to obtain a meaningful comparison of the quadrupole coupling tensors between isotopologues. Furthermore, the impacts of holding an off-diagonal NQCC to a parent value are discussed in further detail for conformer B in Sec. III D 2.

From Table VI, one can see that the experimentally determined value of $\chi_{zz}$ = −73.3(17) MHz is very similar to the value determined for chloromethane, −74.7514(11) MHz[36] by Wlodarczak and co-workers, which we consider an analogue to the chloromethyl group on cyclopropylchloromethyldifluorosilane. Additionally, for the parent species, $|\eta|$ = 0.065(30) and is very small, which suggests that electron density in the C–Cl bond is largely cylindrically symmetrically distributed about the bond. The derived value of $\chi_{zz}$ for 1-chloromethyl-1-fluorosilacyclopentane is −70.6(37) MHz,[6] which is also very similar to that obtained for conformer A, and these two values are within the uncertainty of one another. This suggests that the bonding environments are likely similar (to within experimental uncertainty). Furthermore, the C–Cl bond in conformer A appears largely unaffected by the, presumably, rather electropositive silicon atom in the $-SiF_2-$ unit, adjacent to the chloromethyl moiety. If there were no perturbation of the C–Cl bond at all, one would expect that the value of $\chi_{zz}$ would be identical to that of chloromethane, and this scenario is within the uncertainty of $\chi_{zz}$ for conformer A.

In Table V, the values of $\chi_{zz}$ and $|\eta|$ are collected for a variety of related systems and one can clearly see that the typical value of $\chi_{zz}$ for these molecules ($^{35}$Cl) is around −68 to −76 MHz, and the corresponding values of $|\eta|$ are close to zero. This is further evidence that, despite the unusually small values of the NQCCs (in the PAS) for the parent species of conformer A, these are perfectly reasonable and the derived nature of the electronic environment about the chlorine nucleus, and therefore the nature of the C–Cl bond, is very similar to that in closely related systems.

Additionally, there is very good agreement when one compares the value of $\chi_{zz}$ for the $^{37}$Cl isotopologue of conformer A to that of $CH_3{}^{37}Cl$, where these are −58.61(59) and −58.9116(34) MHz,[36] respectively. Like with the parent species, one can see that the electronic environment about the chlorine nucleus is perturbed little when compared to chloromethane, despite the adjacent $-SiF_2-$ unit, giving further credence to the idea that such a moiety is not having a significant effect on the chlorine-localized electronic environment for this conformation. In Table V, various values of $\chi_{zz}$ for other systems with $^{37}$Cl as the sole quadrupolar nucleus are presented. Like for the $^{35}$Cl species of conformer A, although the NQCCs in the PAS are very small, the value of $\chi_{zz}$ for the $^{37}$Cl isotopologue of conformer A is typical in its magnitude when compared to other systems—particularly so when compared to that of $CH_3{}^{37}Cl$.

When the experimentally determined values of $\chi_{zz}$ and $|\eta|$ are compared with those obtained from quantum chemical calculations in Table VI, the most obvious aspect is striking agreement between the calculated values of $\chi_{zz}$ and $|\eta|$ (for all methods) and the experimental ones, despite the very different values of the NQCCs in the PAS—see Tables II and III. It is acknowledged, however, that the values of $\chi_{zz}$ for the MP2 and QCISD methods fall outside of the uncertainty of the experimental value. (Interestingly, the experimental value of $\chi_{zz}$ is more comparable to that of the CAM-B3LYP calculation rather than that of MP2, which was far superior in predicting the NQCCs in the PAS.) This gives further traction to the idea that, despite the difficulty in resolving the hyperfine structure of conformer A, the experimentally determined NQCCs in the PAS (and thus the electric field gradient at the Cl nucleus) are reasonable. Additionally, one can conclude that the significant differences in the NQCCs in the PAS—particularly those of sign—calculated by the various methods are largely due to subtle differences in geometry and therefore the locations of the principal axes, rather than the inability of any given method to provide an accurate estimation of the electric field about the chlorine atom. Unfortunately, it appears that, for this conformation of cyclopropylchloromethyldifluorosilane, the chlorine atom is located, serendipitously, in a part of the molecule where the electric field gradient at the chlorine atom and along the *a* axis is almost zero, and therefore, the value of $\chi_{aa}$ is prone to vary significantly with subtle changes in the principal axes.

Comparing the value of $\chi_{zz}$ for the parent species to that of the $^{37}$Cl isotopologue (Table VI), a ratio of 1.251(32) is obtained, which is very close to the ratio of the quadrupole moments, *Q*, of $^{35}$Cl and $^{37}$Cl, which is determined to be 1.268 89(3) by Legon and Thorn[37] from analysis of the rotational spectrum of BrCl. It is worth noting that the paper on chloromethane by Wlodarczak and co-workers yields a $Q(^{35}Cl)/Q(^{37}Cl)$ ratio of 1.268 87(8),[36] which they do not explicitly report. The ratio by Wlodarczak *et al.* and that by Legon and Thorn are within uncertainty of one another, so it is inconsequential which ratio is quoted. We continue to reference that of Legon and Thorn as the uncertainty is slightly lower and it is featured in the well-cited summary by Pyykkö.[38]

Given the *z* axes between species are now defined to be the same and isotopic substitution seldom changes the overall electronic or geometric nature of the molecule, the electric field gradients, $q_{zz}$, about the chlorine atom of the two isotopologues should be identical. Therefore, the ratio $\chi_{zz}(^{35}Cl)/\chi_{zz}(^{37}Cl)$, where $\chi_{zz}$ is evaluated as $\chi_{zz} = eQq_{zz}$, should be the same as the ratio $Q(^{35}Cl)/Q(^{37}Cl)$, as *e* is the charge of the electron and is constant. The accepted ratio of Legon and Thorn[37] lies within the uncertainty that is attributed to the experimentally determined ratio, which is obtained by propagating the uncertainties in the values of $\chi_{zz}$ for the appropriate isotopologues. Hence, it can be concluded that the quadrupole coupling tensors for the parent and $^{37}$Cl isotopologues of conformer A are self-consistent, and the change in the sign of $\chi_{aa}$ between the two is genuine, rather than an artifact of the unresolved hyperfine splitting, recalling $\chi_{aa}$ $^{35}$Cl = +0.1393(73) MHz vs $\chi_{aa}$ $^{37}$Cl = −0.8980(93) MHz. This effect is also shown in Table S1(a) of the supplementary material where the transformation of the principal axes, and the change in the quadrupole moment, *Q*, upon substitution of $^{35}$Cl to $^{37}$Cl also leads to a change in the sign of $\chi_{aa}$ as calculated by MP2. It is expected that the ratio $\chi_{zz}(^{35}Cl)/\chi_{zz}(^{37}Cl)$ would be closer to the accepted value and with lower uncertainty were it possible to resolve completely the hyperfine splitting for conformer A.

Comparing now the values of $\chi_{zz}$ of the parent species to those of the $^{29}$Si and $^{30}$Si isotopologues, a ratio about 1.00 is achieved, within the associated uncertainty. This is entirely as expected, given that the quadrupolar nucleus responsible for the

hyperfine structure in the spectrum does not change between these isotopologues. For the doubly substituted isotopologues, two ratios are presented in Table VI: one to the parent species ($^{35}$Cl) and one to the singly substituted $^{37}$Cl isotopologue. The same $\chi_{zz}(^{35}\text{Cl})/\chi_{zz}(^{37}\text{Cl})$ ratio for the doubly substituted $^{37}$Cl–$^{29}$Si isotopologue is achieved, 1.251(29), as is for the singly substituted $^{37}$Cl isotopologue, 1.251(32), and the uncertainty in the former ratio still contains the expected quadrupole moment ratio, $Q(^{35}\text{Cl})/Q(^{37}\text{Cl})$, of 1.268 89(3).[37] The ratio when comparing the values of $\chi_{zz}$ for the $^{37}$Cl–$^{29}$Si and $^{37}$Cl isotopologues is 1.000(10) and is as expected, again, as the quadrupolar nucleus has not changed between these isotopologues. Both of these provide reassurance that the fits for this low-abundance, doubly substituted isotopologue are reasonable. The above is also true for the doubly substituted $^{37}$Cl–$^{30}$Si isotopologue: the $\chi_{zz}(^{35}\text{Cl})/\chi_{zz}(^{37}\text{Cl})$ and $\chi_{zz}(^{37}\text{Cl})/\chi_{zz}(^{37}\text{Cl})$ ratios are 1.250(29) and 1.000(10), respectively, and the uncertainty associated with these contains $Q(^{35}\text{Cl})/Q(^{37}\text{Cl})$ by Legon and Thorn and $Q(^{37}\text{Cl})/Q(^{37}\text{Cl})$, which is one—see Table VI.

### 2. Conformer B

In conformer B, in all but a few cases, the hyperfine splitting of each transition was very well resolved, and this can be seen for *a*- and *b*-type transitions in Fig. 6(b) and contrasted with those for conformer A in Fig. 6(a). The most striking differences between the spectra of the parent species of conformers A and B are that the *a*- and *b*-type transitions are well resolved in the latter, and the magnitude of the splitting of the *c*-type transitions is much greater in conformer B than in conformer A. Notably, the $6_{1,5}\ F' \leftarrow 5_{0,5}\ F''$ transition for the parent species of conformer A is split by less than 1 MHz, peak-to-peak, and the "same" transition in the parent species of conformer B is split by nearly 13 MHz (Fig. 7)—over an order of magnitude of difference. One can see, from Fig. 6(b), that the *a*- and *b*-type transitions for conformer B are split by about 1 MHz, peak-to-peak, compared to conformer A where all four *F*-components of the $\Delta J = +1$ transitions are being predicted (often) to fall within about 200 kHz of one another.

The well-resolved splitting of the hyperfine transitions in conformer B into distinct patterns made the assignment of both isotopologues of this conformation comparatively trivial, and almost all hyperfine transitions were uniquely identifiable for both isotopologues of conformer B. This observation is also reflected in the greater, and more typical, magnitude of $\chi_{aa}$ for the parent species of conformer B, which is +13.9253(80) MHz (Table IV). When compared to that of the parent species of conformer A, where $\chi_{aa}$ = +0.1393(73) MHz, the value of $\chi_{aa}$ for the parent species of conformer B is ~100 times greater. This is also seen for $\chi_{bb} - \chi_{cc}$ (although to a lesser extent), which is −73.137(12) MHz for the parent species in conformer B, vs −4.3320(88) MHz for that of conformer A, although this time, the magnitude of $\chi_{bb} - \chi_{cc}$ is only ~17 times greater for conformer B than it is for conformer A. In addition, the values of $\chi_{aa}$ and $\chi_{bb} - \chi_{cc}$ for the parent species of conformer B are more comparable in magnitude to those determined for the parent species of 1-chloromethyl-1-fluorosilacyclopentane, which were determined to be +16.329(21) and −90.528(48) MHz, respectively.[6] The NQCCs for conformer B are in good agreement with the values predicted by both CAM-B3LYP and MP2, as presented in Table IV.

The $^{37}$Cl isotopologue of conformer B (Table IV) is now considered. Notably, the values of the NQCCs are lower in magnitude than those of the parent. One might generally anticipate this, given $Q(^{37}\text{Cl})$ is smaller than $Q(^{35}\text{Cl})$,[38,39] although conformer A does show that unusual values of $q_{ij}$ can make the NQCCs for $^{35}$Cl smaller in magnitude than those for $^{37}$Cl (Table III), despite a larger quadrupole moment. Nonetheless, it was still possible to resolve a similar, distinct pattern of four $\Delta F = +1$ hyperfine transitions belonging to a single R-branch rotational transition—see, for example, Fig. 7(d).

It was not possible to determine the off-diagonal element, $\chi_{ac}$, and there are two pathways forward from this point: either $\chi_{ac}$ is discounted entirely from the Hamiltonian or it is held to the parent value, divided by 1.268 89,[37] and then truncated to the appropriate number of significant figures. There are strengths and weaknesses to both treatments.

For the former approach, a parameter is not included in the Hamiltonian, which cannot be explicitly determined, is sensitive to any change in the principal axes ($q_{ij}$ will change), and how much this will change cannot be known without measuring it. However, without including $\chi_{ac}$ in some manner, the quadrupole coupling tensor cannot be diagonalized and therefore cannot be compared to conformer A. For conformer B, the MP2 calculation yielded $\chi_{ac}$ as the only negative off-diagonal NQCC. When this parameter is excluded from the tensor, to retain an overall negative sign-product of the off-diagonal elements of the quadrupole coupling tensor, $\chi_{ab}$ is taken to be the singular negative off-diagonal NQCC instead. As noted in Sec. III D 1, the choice of whether to make $\chi_{ab}$ or $\chi_{bc}$ negative is somewhat arbitrary as it is only possible to determine the overall sign-product of the tensor,[34] and even then, it was not possible to determine the overall sign-product in conformer A, given the uncertainty attributed to the line centers—this remains true for conformer B and is kept to be consistent with that predicted by MP2/aug-cc-pVTZ. Furthermore, for symmetry reasons, the off-diagonal part of the quadrupole coupling tensor cannot have only two non-zero elements, so this situation is less physically realistic.[34]

For the latter approach, it is assumed that the principal axes will not change significantly upon substitution of $^{35}$Cl with $^{37}$Cl (this assumption also coincides with a change in quadrupole moment, *Q*), so the value of $\chi_{ac}$ in the quadrupole coupling tensor may not be wholly accurate. However, it is possible to achieve a qualitative comparison of $\chi_{zz}$ and $|\eta|$ between the two isotopologues of conformer B, as well as conformer A and similar molecules (Table V). If one treats $\chi_{ac}$ in this way, it is then held to a value of $\chi_{ac}$ = −10.89 MHz (Table IV), which is very similar to the value calculated by MP2/aug-cc-pVTZ (−10.1650 MHz)—see Table S1(b) of the supplementary material. The other off-diagonal NQCCs (and on-diagonal NQCCs) are calculated well by this method and are thus reassured that the held value of $\chi_{ac}$ is likely close to that which would be determined experimentally, had it been possible to observe more transitions for this isotopologue.

Consequently, and to aid comparison of the above assumptions, both treatments of $\chi_{ac}$ are considered simultaneously, but independently. At this point, it is noted that the MW rms values, and indeed the rest of the determined parameter values (Table IV), are identical (to within the uncertainty in the parameter values) for both treatments for $\chi_{ac}$. This means that these two fits, based on different assumptions of the quadrupole coupling tensor, are essentially the

**TABLE VII.** Nucleus-centered nuclear quadrupole coupling constants (NQCCs) resulting from the diagonalization of the quadrupole coupling tensor for the observed isotopologues of conformer B of cyclopropylchloromethyldifluorosilane.

| | Calculated[a] | | Experimental[b] | | |
|---|---|---|---|---|---|
| | CAM-B3LYP | MP2 | Parent | $^{37}$Cl (no $\chi_{ac}$)[c] | $^{37}$Cl (with $\chi_{ac}$)[c] |
| $\chi_{zz}$[d] (MHz) | −73.5892 | −71.0461 | −76.09(38) | −53.04(76) | −55.89(77) |
| Ratio[e] | ⋯ | ⋯ | ⋯ | 1.435(22) | 1.362(20) |
| $\lvert\eta\rvert$[f] | 0.0083 | 0.0096 | 0.0264(87) | 0.343(12) | 0.071(15) |

[a]The augmented triple-ζ basis set, aug-cc-pVTZ, was used for all atoms in all calculations. The NQCCs are calculated using the $^{35}$Cl isotope.
[b]The value of $\chi_{zz}$ for chloromethane is −74.7514(11)—see Ref. 36.
[c]It was not possible to determine $\chi_{ac}$ for the $^{37}$Cl isotopologue of conformer B. For reasons discussed in the text, two datasets are provided: one where $\chi_{ac}$ is kept out of the quadrupole coupling tensor entirely and one where $\chi_{ac}$, as determined for the parent species, was divided by 1.268 89,[37] and then truncated to the appropriate number of significant figures.
[d]It is assumed that the $z$ axis lies along, or very close to, the Cl–C bond.
[e]This is the ratio of the experimentally determined value of $\chi_{zz}$ to that of the parent. The uncertainty is based on the propagation of the errors in the values of $\chi_{zz}$. The theoretical ratio between the quadrupole moments, $Q$, of atomic chlorine, $Q(^{35}\text{Cl})$ and $Q(^{37}\text{Cl})$ should be ~1.268 89(3)[37,38]—see the text for commentary.
[f]This is a measure of the asymmetry of the electric field gradient along the $z$ axis, $\eta = \frac{\chi_{xx}-\chi_{yy}}{\chi_{zz}}$. A value of zero indicates perfect cylindrical symmetry.

same: the assumed value of $\chi_{ac}$ is not detrimental to the fit, but, equally, it is not possible to be certain of its true value with the data available. Both treatments have their own strengths and weaknesses as discussed above, and we have no preference for either, given that the resulting fits are almost identical, but both fits are useful for different reasons.

Considering now the diagonalized quadrupole coupling tensor of the parent species for conformer B, one can see from Table VII that $\chi_{zz}$ and $|\eta|$ are in good agreement with the calculated values and notably more certain than was the case for conformer A. In addition, the value of $\chi_{zz}$ for the parent species of conformer B, −76.09(38) MHz, is larger than that for the parent species of conformer A, −73.3(17) MHz, even when one considers the large uncertainty in the latter value. The reason for this is unclear, but may arise owing to a subtle geometry-induced difference in how chloromethyl moiety is interacting with the rest of the molecule, highlighting, in particular, the difference of location of the chlorine atom with respect to the cyclopropyl ring between the two conformations (see Fig. 2). Despite this, it is noted that the value of $\chi_{zz}$ for conformer B is similar to that of chloromethane, −74.7514(11),[36] but this time, it is more different to that of 1-chloromethyl-1-fluorosilacyclopentane, −70.6(37) MHz,[6] even when the large uncertainty of the latter is considered.

Furthermore, looking at the values of $|\eta|$ between conformers A and B (Table V), these indicate an approximately equal degree of cylindrical symmetry in the electron density about the $z$ axis, when one considers the uncertainties on both values. This is largely as expected as one would not expect the bonding environment to change significantly upon rotation of the chloromethyl group, especially given the geometric arguments made in previous Sec. III A.

In comparison to the $\chi_{zz}(^{35}\text{Cl})/\chi_{zz}(^{37}\text{Cl})$ ratio for conformer A (Table VI), the ratios achieved from this analysis for conformer B (Table VII), for both treatments of $\chi_{ac}$, are further away from that expected.[37] We believe these mismatching ratios are a result of the assumptions made about the value of $\chi_{ac}$, rather than any inherent inadequacy with the determined spectroscopic constants in Table IV, rendering the values of $\chi_{zz}$ and $|\eta|$ somewhat more qualitative for conformer B than for conformer A. As a value of $\chi_{ac}$ is required to diagonalize the quadrupole coupling tensor, in the case where $\chi_{ac}$ is excluded from the Hamiltonian entirely, it must be assumed to be zero. This results in a large degree of asymmetry in the electric field gradient about the C–Cl bond (and is reflected in the unreasonable value of $|\eta|$), and this leads to an unreliable value of $\chi_{zz}$ as the off-diagonal part of the quadrupole coupling tensor is not physically meaningful. This returns a greater-than-expected $\chi_{zz}(^{35}\text{Cl})/\chi_{zz}(^{37}\text{Cl})$ ratio of 1.435(22), when compared to the expected 1.268 89(3).[37] When $\chi_{ac}$ is held to the parent value, divided by the ratio in Ref. 37, it is assumed that the principal axes, and therefore $q_{ij}$, do not change significantly. While this was a reasonable assumption for silicon in Sec. III D 1, this is not as appropriate for the chlorine atom in this instance. While the change in mass between $^{35}$Cl and $^{37}$Cl is approximately the same as that between $^{28}$Si and $^{30}$Si (~2 $m_u$), the difference this time is the location of the atom in the molecule. The silicon atom in conformer A is located very close to the center of mass; therefore, isotopic substitution is likely to have a minimal effect on the principal axes, whereas here the chlorine atom is much further away from the center of mass, so such substitution will have a larger effect on the principal axes and therefore $q_{ij}$ and the NQCCs in the PAS (see Fig. 4). This, then, maybe the primary reason for the $\chi_{zz}(^{35}\text{Cl})/\chi_{zz}(^{37}\text{Cl})$ ratio, in Table VII, to be higher than expected, at 1.362(20).

### E. Observation of electric dipole forbidden transitions in the rotational spectra of the $^{37}$Cl isotopologue of conformer A and the parent isotopologue of conformer B

One of the more interesting aspects of the rotational spectra of the $^{37}$Cl isotopologue of conformer A, and the parent isotopologue of conformer B, is the observation of nine (total) electric dipole forbidden transitions. These are listed in Table VIII.

**TABLE VIII.** A list of the electric dipole forbidden, quadrupole allowed transitions observed in the rotational spectra of the $^{37}$Cl isotopologue of conformer A and the parent species of conformer B.

| Number | $J'_{K'_a,K'_c}F' \leftarrow J''_{K''_a,K''_c}F''$ | Frequency (MHz) |
|---|---|---|
| | Conformer A—$^{37}$Cl | |
| 1 | $8_{1,7}\ \frac{13}{2} \leftarrow 6_{4,3}\ \frac{11}{2}$ | 12 532.2247 |
| 2 | $8_{1,7}\ \frac{17}{2} \leftarrow 6_{4,3}\ \frac{15}{2}$ | 12 532.2247 |
| 3 | $7_{4,4}\ \frac{13}{2} \leftarrow 7_{2,6}\ \frac{11}{2}$ | 13 080.8316 |
| 4 | $7_{4,4}\ \frac{17}{2} \leftarrow 7_{2,6}\ \frac{15}{2}$ | 13 081.0219 |
| | Conformer B—parent | |
| 5 | $5_{1,4}\ \frac{7}{2} \leftarrow 3_{3,0}\ \frac{5}{2}$ | 13 160.6164 |
| 6 | $5_{1,4}\ \frac{11}{2} \leftarrow 3_{3,0}\ \frac{9}{2}$ | 13 166.3297 |
| 7 | $5_{1,4}\ \frac{7}{2} \leftarrow 3_{3,1}\ \frac{7}{2}$ | 13 178.2334 |
| 8 | $6_{2,4}\ \frac{9}{2} \leftarrow 4_{4,0}\ \frac{7}{2}$ | 15 158.4112 |
| 9 | $5_{5,0}\ \frac{9}{2} \leftarrow 5_{1,4}\ \frac{7}{2}$ | 16 647.0067 |

It was not possible to differentiate between the two different $F$ components of the $c$-type $\Delta J = +2$ transitions for the $^{37}$Cl isotopologue of conformer A (labeled as transitions 1 and 2 in Table VIII) as their predicted intensities were virtually identical, and they were both predicted to lie below the same line. Therefore, these two transitions were fit together. Additionally, numerous forbidden transitions are predicted to be of considerable intensity (based on the spectroscopic constants and calculated dipole moments in Table IV) for the $^{37}$Cl isotopologue of conformer B; however, these have not been experimentally observed in the rotational spectrum as it was only possible to observe the most intense $c$-type transitions. Therefore, this is not considered any further. Moreover, all electric dipole forbidden transitions were checked against all observed and predicted transitions for the other isotopologues of conformer A, and also those of the $^{37}$Cl isotopologue of conformer B, to ensure these transitions could not be reasonably assigned to anything else. We are also confident that these transitions do not belong to any unidentified conformation in the free-jet expansion (such as conformer C briefly discussed in Sec. III A).

Since electric dipole forbidden, quadrupole allowed transitions were first theorized by Javan[40] in the context of constructing a three-level maser in 1957 and first observed by Oka[41] in ethyl iodide in 1966, the theory has developed such that one can think of a typical electric dipole forbidden transition becoming weakly allowed through the mixing of the wavefunctions of near-degenerate rotational states, facilitated by (typically) an off-diagonal element of the nuclear quadrupole coupling tensor (see, for example, Refs. 42–45 and references therein). As a result, work has largely focused on brominated and iodated systems owing to the lower rotational constants, which increases the density of states at lower internal energies. Furthermore, the large quadrupole moments of the Br and I atoms serve to couple the rotational states more strongly, even at greater energetic separations. These features make electric dipole forbidden, quadrupole allowed transitions more likely to appear, although merely meeting these criteria does not guarantee one will observe electric dipole forbidden transitions. This does mean, however, that electric dipole forbidden, quadrupole allowed transitions are unusual in chlorine-containing species. As such, only two other systems are known to the authors that exhibit them: chlorine nitrate, as studied by Müller and co-workers,[46] and *cis*-1-chloro-2-fluoroethylene, as studied by Dore *et al.*[47]

For the $x$-type transitions, where there is no change in parity of the $K_a$ or $K_c$ quantum numbers, it can be more difficult to explain the mechanisms that give rise to their intensity. As such, there have been only a handful of papers mentioning them (but those that do involve a large amplitude motion,[48,49] a large Coriolis coupling,[50] or a large quadrupole moment[51–54]), and to our knowledge, there have been no publications reporting quadrupole allowed $x$-type transitions in a chlorine-containing molecule. Owing to a combination of the paucity of experimental data on $x$-type transitions in chlorine containing species and the complexity of the underlying interactions that facilitate these transitions, we elect to address this in detail in a forthcoming publication.[55]

Interestingly, despite the off-diagonal NQCCs being larger in magnitude for the parent species of conformer A than for the corresponding $^{37}$Cl isotopologue (see Table III), no electric dipole forbidden transitions are observed for that species (although a handful are very weakly predicted in the 0–25 GHz range over which transitions were predicted). Therefore, the appearance of such transitions in the $^{37}$Cl isotopologue may be as a result of a change in the energies of the rotational states as the mass of the molecule, and the locations of the principal axes, changes. This may allow the states involved in inducing the forbidden transitions to become more strongly mixed by off-diagonal components of the quadrupole coupling tensor, where the corresponding NQCCs are smaller in magnitude.

### F. Experimental substitution ($r_s$) structure

Owing to having fits for various isotopologues in their natural abundances in the free-jet expansion, it is possible to determine a partial substitution structure ($r_s$) for conformer A. The determined geometric parameters, and their values, are presented in Table IX. A table of the atomic coordinates (in the PAS) determinable from the available isotopologue data is given in Table S2(a) of the supplementary material, alongside those calculated using MP2/aug-cc-pVTZ—see Table S2(b) of the supplementary material. For conformer B, only the $^{37}$Cl isotopologue was observed in the rotational spectrum, and therefore, no substitution structure could be obtained; however, it was possible to determine the atomic coordinates of Cl (in the PAS), and these are given in Table S2(c) of the supplementary material.

Briefly, the positions of the heavy atoms are calculated using Kraitchman's equations,[56] as implemented in Kisiel's KRA program.[35] Only the rotational constants of the pertinent isotopologues (and differences in mass with respect to the parent) are required to generate a substitution structure, and therefore, the errors in the rotational constants are propagated into the errors in the resultant coordinates and are given according to the criteria of Costain.[57] As is common knowledge, this process cannot obtain the signs of the coordinates, solely their magnitudes. As such, the signs of the coordinates are assumed from the MP2 $r_e$ structure. An additional pitfall that exists with Kraitchman analysis is that when an atom is close to a principal axis, the position can be difficult to determine

**TABLE IX.** Experimentally determined substitution structure ($r_s$) parameters, and their values, for conformer A of cyclopropylchloromethyldifluorosilane compared to the corresponding theoretical equilibrium structure ($r_e$) parameter values.[a,b]

| | Theoretical ($r_e$)[c] | | | |
|---|---|---|---|---|
| | CAM-B3LYP | QCISD | MP2 | Experimental ($r_s$)[d] |
| $r$(Cl–$C_4$) (Å) | 1.800 | 1.803 | 1.795 | 1.783(11) |
| $r$($C_4$–$^{29}$Si) (Å)<br>$r$($C_4$–$^{30}$Si) (Å) | 1.866 | 1.872 | 1.871 | 1.861(20)<br>1.861(20) |
| $r$($^{29}$Si–$C_3$) (Å)<br>$r$($^{30}$Si–$C_3$) (Å) | 1.824 | 1.829 | 1.826 | 1.811(11)<br>1.811(11) |
| $\theta$(Cl–$C_4$–$^{29}$Si) (deg)<br>$\theta$(Cl–$C_4$–$^{30}$Si) (deg) | 109.65 | 108.50 | 107.64 | 108.20(96)<br>108.20(98) |
| $\theta$($C_4$–$^{29}$Si–$C_3$) (deg)<br>$\theta$($C_4$–$^{30}$Si–$C_3$) (deg) | 116.23 | 115.19 | 114.56 | 114.13(50)<br>114.13(51) |
| $\phi$(Cl–$C_4$–$^{29}$Si–$C_3$) (deg)<br>$\phi$(Cl–$C_4$–$^{30}$Si–$C_3$) (deg) | 55.3 | 54.8 | 54.1 | 56.0(18)<br>56.0(18) |

[a]Bond lengths are denoted in the usual manner, $r$, bond angles are represented by $\theta$, and dihedral angles are indicated using $\phi$. The carbon atoms are numbered as in Figs. 2 and 3.
[b]Data are presented pertaining to the substitution of $^{28}$Si with both $^{29}$Si and $^{30}$Si, acknowledging that these should yield the same results within the attributed uncertainty—see the text for commentary.
[c]The augmented triple-ζ basis set, aug-cc-pVTZ, was used for all atoms in all calculations.
[d]Numbers in brackets are the Costain errors,[57] pertaining to the least significant figures, truncated to two significant figures.

from Kraitchman's equations and an imaginary coordinate may occur.[56–60] In the case of conformer A, the silicon atom lies close to the $c$ axis (see Fig. 3), and therefore, the $c$-coordinate was imaginary when substituting both $^{29}$Si and $^{30}$Si; here, it is assumed that the imaginary $c$-coordinate of the silicon atom is zero, although the (rather large) uncertainties in the positions were retained. While the doubly substituted $^{37}$Cl–$^{29}$Si and $^{37}$Cl–$^{30}$Si isotopologues are observed, it was not possible to determine a real $c$-coordinate for the silicon atom, regardless of what species was taken to be the "parent species" for the purposes of Kraitchman substitution. This precludes the use of Rudolph's method of double substitution,[60] which can be useful to elucidate the coordinates of the atoms when Kraitchman's equations fail to yield a real coordinate, provided that, of course, one can obtain a real coordinate for the atom under consideration from the doubly substituted isotopologue.

Once the coordinates of the atoms have been determined, it is then possible to work out the values of geometric parameters, such as bond lengths, bond angles, and dihedral angles. For this, Kisiel's EVAL program[35] was used, and the pertinent, evaluated, geometric parameters obtained are given in Table IX. Therein, the $r_s$ structural parameters are presented based on the substitution of both $^{29}$Si and $^{30}$Si. As isotopic substitution seldom changes the geometry, only the locations of the principal axes, it is expected that the geometric parameter values obtained from these two sets of rotational constants would be identical. This is indeed the case for all parameters. Therefore, the substitution structures when using the rotational constants of $^{29}$Si or $^{30}$Si serve to support the accuracy of those rotational constants.

As one can see from Table IX, the experimental $r_s$ structure is in excellent agreement with the $r_e$ structures, as predicted by both DFT (CAM-B3LYP) and *ab initio* (QCISD and MP2) methods, although the agreement is particularly good with that predicted by MP2. The experimentally determined bond lengths are within ~0.02 Å of the theoretical $r_e$ bond lengths, and both the bond angles and dihedral angles are within ~2° of the theoretical structures. The Cl–$C_4$–Si–$C_3$ dihedral angle is experimentally determined to be 56.0(18)°, regardless of whether one chooses $^{29}$Si or $^{30}$Si. This is in line with the calculated values of 55.3° and 54.1° of CAM-B3LYP and MP2, respectively, and suggests that the isotopologues included in defining this dihedral angle do, indeed, all belong to conformer A. The uncertainty of this value is large in comparison to that in the bond lengths and bond angles, and this is ascribable to there being four atoms that define a dihedral angle, each with its own uncertainty in its position, which, in turn, is determined from the uncertainties in the rotational constants; moreover, the uncertainty on the position of the silicon atom is larger than the others, given that the atom is close to the $c$ axis—see Table S2(a) of the supplementary material.

Such good agreement with the theoretical $r_e$ structures allows us to draw a number of conclusions: first, the assumption that the $c$-coordinate of the silicon atom is zero is reasonable; second, this is further evidence that the rotational constants determined are reasonable for all isotopologues belonging to conformer A; and finally, that computationally inexpensive DFT methods are adequate for obtaining geometric data (although even small differences in the geometry can have a detrimental effect on the quality of the NQCCs in the PAS—see Sec. III D 1).

Finally, the value of $r$(C–Cl) for conformer A is highly comparable to that in chloromethane and is shown, in Table IX, to be 1.783(11) Å, whereas the equivalent $r_0$ parameter value for chloromethane has been determined to be 1.7854(10) Å.[61] This $r_0$ value lies within the uncertainty attributed to the $r_s$ value for cyclopropylchloromethyldifluorosilane (Table IX), which further implies that the nearby –$SiF_2$– unit is not strongly affecting the chloromethyl group, despite the two fluorine atoms being strongly electron withdrawing, and the anticipated large positive charge on the silicon atom. This is in line with conclusions drawn in Sec. III D 1 from analysis of the NQCCs.

## IV. CONCLUSIONS AND CLOSING REMARKS

We have synthesized, recorded, and analyzed the rotational spectrum of, cyclopropylchloromethyldifluorosilane, $c$-$C_3H_5SiF_2CH_2Cl$ and report the experimentally determined spectroscopic constants for two unique conformations, alongside eight associated minor isotopologues. We determine the on-diagonal and all off-diagonal NQCCs for the parent species of both conformers A and B and also the $^{37}$Cl isotopologue for conformer A. Determining a full quadrupole coupling tensor for the $^{37}$Cl isotopologue of conformer B was not possible, but we were able to determine $\chi_{ab}$ and $\chi_{bc}$. Observing $^{37}$Cl, $^{29/30}$Si, and some $^{13}$C isotopologues allowed for the determination of a partial substitution structure ($r_s$) for conformer A. This was not possible for conformer B, whose population in the free-jet expansion was too low to permit the observation of any minor isotopologues other than $^{37}$Cl, with the number of FIDs acquirable, given the limited quantity of samples available.

The quadrupole coupling tensors, in the PASs, of both conformations are interesting, but for different reasons. For conformer A, the values of $\chi_{aa}$ were unusually small and therefore difficult to determine, for all isotopologues, however particularly so for those containing $^{35}$Cl, owing to the unresolved hyperfine splitting. The determined value of $\chi_{aa}$ for the parent species of conformer A is very close to being zero at only $\chi_{aa}$ = +0.1393(73) MHz, and there is a change in sign between this and the corresponding value for the $^{37}$Cl isotopologue, which is determined as $\chi_{aa}$ = −0.8980(93)—the latter is still very small for a chlorine-containing molecule. For the parent species of conformer B, a number of electric dipole forbidden, quadrupole allowed transitions are observed in the rotational spectrum—including those of $x$-type (to be addressed in a forthcoming publication[55]). Electric dipole forbidden transitions were also observed in the rotational spectrum of the $^{37}$Cl isotopologue of conformer A.

Despite the value of $\chi_{aa}$ being small (and therefore difficult to determine from the poorly resolved hyperfine splitting) for conformer A, diagonalizing the quadrupole coupling tensor into a nucleus-centered axis scheme was enlightening. Comparing the experimental value of $\chi_{zz}$ with those calculated by various DFT and *ab initio* methods suggests that the experimentally determined NQCCs are reasonable, in light of the significant variation between the experimental and calculated NQCCs in the PAS; the experimental value of $\chi_{zz}$ was also comparable to similar systems, notably chloromethane[36] and 1-chloromethyl-1-fluorosilacyclopentane.[6] Furthermore, the ratio $Q(^{35}\text{Cl})/Q(^{37}\text{Cl})$, as determined in Ref. 37, lies firmly within the uncertainty attributed to the $\chi_{zz}(^{35}\text{Cl})/\chi_{zz}(^{37}\text{Cl})$ ratio. These points give further credence to the accuracy and reliability of the determined values of the NQCCs, particularly $\chi_{aa}$, for the parent species of conformer A, despite the small magnitude and change in sign between this and the corresponding $^{37}$Cl isotopologue.

The calculated NQCCs in the PAS varied significantly between methods—indeed, only MP2 correctly determined the sign of $\chi_{aa}$. Normally, one method obtaining a different sign for a parameter value, when compared to multiple other quantum chemical methods, would be indicative of a bad geometry, or a method-dependent difficulty in calculating an accurate electric field, or a combination of both. However, the calculated $r_e$ geometry is in excellent agreement with the experimentally determined $r_s$ structure, alongside the diagonalized quadrupole coupling constants ($\chi_{zz}$ and $|\eta|$), which agree well with those determined experimentally. These points are also true for the QCISD and CAM-B3LYP methods; hence, we conclude that, overall, the calculated geometries and electric field gradients for all methods are reasonable (noting that is useful to correct for long-range interactions for B3LYP), and it is the very subtle differences in the geometries that lead to very subtle differences in the principal axes, which makes the evaluation of the NQCCs in the PAS difficult. This is primarily because of the quadrupolar nucleus being located, serendipitously, in a part of the molecule where the electric field gradient, measured at the chlorine nucleus, is particularly small along the $a$ axis. Therefore, it is imperative that one looks at the electric field gradient as a whole, when centered at the quadrupolar nucleus, rather than individual components of it projected onto the principal axes, to determine if the calculated electric field gradient about a quadrupolar nucleus is reasonable. However, it is accepted that it is this projection of the electric field gradient onto the principal axes that determines the extent of the hyperfine splitting in the rotational spectrum of a molecule. That the value of $\chi_{aa}$ is particularly small in conformer A is supported by the majority of transitions having unresolved, or partially resolved, hyperfine structures.

While the *ab initio* MP2 method (with the aug-cc-pVTZ basis set) yielded the most accurate rotational constants, NQCCs in the PAS and geometry when compared to the experimentally determined values (for both conformers A and B), it is somewhat difficult to say that this would be the best method to use for related systems. This is a comparatively simple method to determine the electronic structure of molecules and the more complex QCISD method predicted NQCCs that were not in good agreement with the experiment (but still very reasonable nonetheless). This leads us to believe that the accuracy of MP2, in this case, is somewhat fortuitous, rather than any systematic result of the way in which this method works. It would be interesting to see how a geometry and NQCCs calculated using the CCSD(T) method would compare to those of the QCISD and MP2 methods and the experiment, although this would be an incredibly, perhaps prohibitively, computationally expensive task.

## SUPPLEMENTARY MATERIAL

Complete lists of transitions for all observed isotopologues of both conformations are made available in the supplementary material, alongside the results of transforming the calculated data into new sets of principal axes for various isotopologues and the

determinable atomic coordinates (in the principal axis system) obtained from Kraitchman substitution. The NMR spectra obtained after the synthesis of cyclopropylchloromethyldifluorosilane are also provided.

## ACKNOWLEDGMENTS

This work was supported by the National Science Foundation, United States, under Grant No. CHE-MRI-2019072. A.R.D. and G.S.G. II are also grateful for access to the high-performance computing facility, The Foundry, at the Missouri University of Science and Technology, which was supported by the National Science Foundation under Grant No. OAC-1919789. A.G.H. acknowledges a Major Academic Year Support (MAYS) grant from the College of Charleston for the year 2022–2023.

## AUTHOR DECLARATIONS

### Conflict of Interest

The authors have no conflicts to disclose.

### Author Contributions

**Alexander R. Davies**: Data curation (equal); Formal analysis (equal); Investigation (equal); Validation (equal); Visualization (equal); Writing – original draft (equal); Writing – review & editing (equal). **Abanob G. Hanna**: Data curation (equal); Formal analysis (equal); Investigation (equal); Validation (equal); Writing – review & editing (equal). **Alma Lutas**: Data curation (equal); Formal analysis (equal); Investigation (equal); Validation (equal); Writing – review & editing (equal). **Gamil A. Guirgis**: Conceptualization (equal); Data curation (equal); Formal analysis (equal); Funding acquisition (equal); Investigation (equal); Methodology (equal); Project administration (equal); Resources (equal); Supervision (equal); Validation (equal); Writing – review & editing (equal). **G. S. Grubbs II**: Conceptualization (equal); Data curation (equal); Formal analysis (equal); Funding acquisition (equal); Investigation (equal); Methodology (equal); Project administration (equal); Resources (equal); Supervision (equal); Validation (equal); Writing – review & editing (equal).

## DATA AVAILABILITY

The data that support the findings of this study are available within the article and its supplementary material.

## REFERENCES

[1]T. M. C. McFadden, F. E. Marshall, E. J. Ocola, J. Laane, G. A. Guirgis, and G. S. Grubbs II, "Theoretical calculations, microwave spectroscopy, and ring-puckering vibrations of 1,1-dihalosilacyclopent-2-enes," J. Phys. Chem. A **124**(40), 8254–8262 (2020).

[2]L. Licaj, N. Moon, G. S. Grubbs II, G. A. Guirgis, and N. A. Seifert, "Broadband microwave spectroscopy of cyclopentylsilane and 1,1,1-trifluorocyclopentylsilane," J. Mol. Spectrosc. **390**, 111698 (2022).

[3]N. T. Moon, F. E. Marshall, T. M. C. McFadden, E. J. Ocola, J. Laane, G. A. Guirgis, and G. S. Grubbs II, "Pure rotational spectrum and structural determination of 1,1-difluoro-1-silacyclopentane," J. Mol. Struct. **1249**, 131563 (2022).

[4]T. M. C. McFadden, N. Moon, F. E. Marshall, A. J. Duerden, E. J. Ocola, J. Laane, G. A. Guirgis, and G. S. Grubbs II, "The molecular structure and curious motions in 1,1-difluorosilacyclopent-3-ene and silacyclopent-3-ene as determined by microwave spectroscopy and quantum chemical calculations," Phys. Chem. Chem. Phys. **24**(4), 2454–2464 (2022).

[5]A. Jabri, F. E. Marshall, W. R. N. Tonks, R. E. Brenner, D. J. Gillcrist, C. J. Wurrey, I. Kleiner, G. A. Guirgis, and G. S. Grubbs II, "The conformational landscape, internal rotation, and structure of 1,3,5-trisilapentane using broadband rotational spectroscopy and quantum chemical calculations," J. Phys. Chem. A **124**(19), 3825–3835 (2020).

[6]T. Pulliam, F. E. Marshall, T. Carrigan-Broda, D. V. Hickman, G. Guirgis, and G. S. Grubbs II, "The chirped pulse, Fourier transform microwave spectrum of 1-chloromethyl-1-fluorosilacyclopentane," J. Mol. Spectrosc. **395**, 111793 (2023).

[7]N. T. Moon, A. J. Duerden, T. M. C. McFadden, N. A. Seifert, G. A. Guirgis, and G. S. Grubbs II, "Rotational spectrum and ring structures of silacyclohex-2-ene and 1,1-difluorosilacyclohex-2-ene," J. Phys. Chem. A **128**, 10–19 (2023).

[8]J. R. Glenn, J. E. Isert, J. D. Bethke, G. A. Guirgis, and G. S. Grubbs II, "The microwave spectrum of the low energy conformers of 1-ethylsilacyclopentane," J. Mol. Spectrosc. **399**, 111872 (2023).

[9]R. H. Schwendeman and G. D. Jacobs, "Microwave spectrum, structure, quadrupole coupling constants, and barrier to internal rotation of chloromethylsilane," J. Chem. Phys. **36**(5), 1251–1257 (1962).

[10]R. H. Schwendeman, G. D. Jacobs, and T. M. Krigas, "Molecular structure of cyclopropyl chloride," J. Chem. Phys. **40**(4), 1022–1028 (1964).

[11]F. G. Fujiwara, J. C. Chang, and H. Kim, "Microwave spectrum and rotational isomers of cyclopropylcarbinyl chloride and epichlorohydrin," J. Mol. Struct. **41**(2), 177–182 (1977).

[12]M. A. Mohammadi and W. V. F. Brooks, "The microwave spectrum and structure of chloromethyl cyclopropane," J. Mol. Spectrosc. **73**(3), 347–352 (1978).

[13]N. Heineking, J.-U. Grabow, and I. Merke, "Molecular beam Fourier transform microwave spectra of (chloromethyl)cyclopropane and (chloromethyl)oxirane," J. Mol. Struct. **612**(2–3), 231–244 (2002).

[14]S. S. Panikar, G. A. Guirgis, M. T. Eddens, H. W. Dukes, A. R. Conrad, M. J. Tubergen, T. K. Gounev, and J. R. Durig, "Microwave, infrared and Raman spectra, adjusted $r_0$ structural parameters, conformational stability, and vibrational assignment of cyclopropylfluorosilane," Chem. Phys. **415**, 124–132 (2013).

[15]T. K. Gounev, S. W. Hur, M. Dakkouri, A. Grunvogel-Hurst, and J. R. Durig, "Infrared and Raman spectra, conformational stability, *ab initio* calculations, and vibrational assignments for cyclopropyldifluorosilane," Struct. Chem. **9**(2), 95–112 (1998).

[16]T. K. Gounev, J. W. Weston, S. Shen, M. Dakkouri, A. Grunvogel-Hurst, and J. R. Durig, "Infrared and Raman spectra, conformational stability, *ab initio* calculations, and vibrational assignments for cyclopropylchlorosilane," J. Phys. Chem. A **101**(46), 8614–8624 (1997).

[17]S. W. Hur, "Conformational stability studies by variable temperature infrared spectra of rare gas solutions and *ab initio* calculations of some substituted three-membered ring compounds and ethylene molecules," Ph.D. thesis, University of Missouri, Kansas City, 2001.

[18]M. D. Foellmer, J. M. Murray, M. M. Serafin, A. L. Steber, R. A. Peebles, S. A. Peebles, J. L. Eichenberger, G. A. Guirgis, C. J. Wurrey, and J. R. Durig, "Microwave spectra and barrier to internal rotation in cyclopropylmethylsilane," J. Phys. Chem. A **113**(21), 6077–6082 (2009).

[19]J. R. Durig, S. S. Panikar, G. A. Guirgis, T. K. Gounev, R. M. Ward, R. A. Peebles, S. A. Peebles, R. J. Liberatore, S. Bell, and C. J. Wurrey, "Conformational stability, $r_0$ structural parameters, barriers to internal rotation, vibrational spectra and *ab initio* calculations of c-$C_3H_5SiH_2CH_3$," J. Mol. Struct. **923**(1–3), 1–12 (2009).

[20]R. E. Dorris, B. C. Luce, S. J. Stettner, R. A. Peebles, S. A. Peebles, J. L. Bullard, J. E. Bunn, and G. A. Guirgis, "Effect of fluorination on methyl internal rotation barriers: Microwave spectra of cyclopropylfluoromethyl silane ($c$-$C_3H_5SiHFCH_3$) and cyclopropyldifluoromethyl silane ($c$-$C_3H_5SiF_2CH_3$)," J. Mol. Spectrosc. **318**, 101–106 (2015).

[21]A. Duerden, F. E. Marshall, N. Moon, C. Swanson, K. M. Donnell, and G. S. Grubbs II, "A chirped pulse Fourier transform microwave spectrometer with multi-antenna detection," J. Mol. Spectrosc. **376**, 111396 (2021).
[22]F. E. Marshall, D. J. Gillcrist, T. D. Persinger, S. Jaeger, C. C. Hurley, N. E. Shreve, N. Moon, and G. S. Grubbs II, "The CP-FTMW spectrum of bromoperfluoroacetone," J. Mol. Spectrosc. **328**, 59–66 (2016).
[23]G. Sedo, F. E. Marshall, and G. S. Grubbs II, "Rotational spectra of the low energy conformers observed in the (1R)-(−)-myrtenol monomer," J. Mol. Spectrosc. **356**, 32–36 (2019).
[24]Z. Kisiel and J. Kosarzewski, "Identification of trace 2-chloropropene with a new chirped pulse microwave spectrometer," Acta Phys. Pol., A **131**(2), 311–317 (2017).
[25]H. M. Pickett, "The fitting and prediction of vibration-rotation spectra with spin interactions," J. Mol. Spectrosc. **148**(2), 371–377 (1991).
[26]Z. Kisiel, L. Pszczółkowski, I. R. Medvedev, M. Winnewisser, F. C. De Lucia, and E. Herbst, "Rotational spectrum of *trans–trans* diethyl ether in the ground and three excited vibrational states," J. Mol. Spectrosc. **233**(2), 231–243 (2005).
[27]C. M. Western, "PGOPHER: A program for simulating rotational, vibrational and electronic spectra," J. Quant. Spectrosc. Radiat. Transfer **186**, 221–242 (2017).
[28]M. J. Frisch, G. W. Trucks, H. B. Schlegel, G. E. Scuseria, M. A. Robb, J. R. Cheeseman, G. Scalmani, V. Barone, G. A. Petersson, H. Nakatsuji, X. Li, M. Caricato, A. V. Marenich, J. Bloino, B. G. Janesko, R. Gomperts, B. Mennucci, H. P. Hratchian, J. V. Ortiz, A. F. Izmaylov, J. L. Sonnenberg, D. Williams-Young, F. Ding, F. Lipparini, F. Egidi, J. Goings, B. Peng, A. Petrone, T. Henderson, D. Ranasinghe, V. G. Zakrzewski, J. Gao, N. Rega, G. Zheng, W. Liang, M. Hada, M. Ehara, K. Toyota, R. Fukuda, J. Hasegawa, M. Ishida, T. Nakajima, Y. Honda, O. Kitao, H. Nakai, T. Vreven, K. Throssell, J. A. Montgomery, Jr., J. E. Peralta, F. Ogliaro, M. J. Bearpark, J. J. Heyd, E. N. Brothers, K. N. Kudin, V. N. Staroverov, T. A. Keith, R. Kobayashi, J. Normand, K. Raghavachari, A. P. Rendell, J. C. Burant, S. S. Iyengar, J. Tomasi, M. Cossi, J. M. Millam, M. Klene, C. Adamo, R. Cammi, J. W. Ochterski, R. L. Martin, K. Morokuma, O. Farkas, J. B. Foresman, and D. J. Fox, *GAUSSIAN 16, Revision C.01*, 2016.
[29]H.-J. Werner, P. J. Knowles, P. Celani, W. Györffy, A. Hesselmann, D. Kats, G. Knizia, A. Köhn, T. Korona, D. Kreplin, R. Lindh, Q. Ma, F. R. Manby, A. Mitrushenkov, G. Rauhut, M. Schütz, K. R. Shamasundar, T. B. Adler, R. D. Amos, S. J. Bennie, A. Bernhardsson, A. Berning, J. A. Black, P. J. Bygrave, R. Cimiraglia, D. L. Cooper, D. Coughtrie, M. J. O. Deegan, A. J. Dobbyn, K. Doll, M. Dornbach, F. Eckert, S. Erfort, E. Goll, C. Hampel, G. Hetzer, J. G. Hill, M. Hodges, T. Hrenar, G. Jansen, C. Köppl, C. Kollmar, S. J. R. Lee, Y. Liu, A. W. Lloyd, R. A. Mata, A. J. May, B. Mussard, S. J. McNicholas, W. Meyer, T. F. Miller III, M. E. Mura, A. Nicklass, D. P. O'Neill, P. Palmieri, D. Peng, K. A. Peterson, K. Pflüger, R. Pitzer, I. Polyak, M. Reiher, J. O. Richardson, J. B. Robinson, B. Schröder, M. Schwilk, T. Shiozaki, M. Sibaev, H. Stoll, A. J. Stone, R. Tarroni, T. Thorsteinsson, J. Toulouse, M. Wang, M. Welborn, and B. Ziegler, MOLPRO, version 2021.2, a package of *ab initio* programs, 2021.
[30]W. R. Shields, T. J. Murphy, E. L. Garner, and V. H. Dibeler, "Absolute isotopic abundance ratio and the atomic weight of chlorine," J. Am. Chem. Soc. **84**(9), 1519–1522 (1962).
[31]S. Grimme, J. Antony, S. Ehrlich, and H. Krieg, "A consistent and accurate *ab initio* parametrization of density functional dispersion correction (DFT-D) for the 94 elements H-Pu," J. Chem. Phys. **132**(15), 154104 (2010).
[32]E. R. Johnson and A. D. Becke, "A post-Hartree-Fock model of intermolecular interactions: Inclusion of higher-order corrections," J. Chem. Phys. **124**(17), 174104 (2006).
[33]T. Yanai, D. P. Tew, and N. C. Handy, "A new hybrid exchange–correlation functional using the Coulomb-attenuating method (CAM-B3LYP)," Chem. Phys. Lett. **393**(1–3), 51–57 (2004).
[34]U. Spoerel, H. Dreizler, and W. Stahl, "Notizen: On the sign of the off-diagonal elements of the nuclear quadrupole coupling tensor," Z. Naturforsch., A **49**(4–5), 645–646 (1994).
[35]Z. Kisiel, Programs for ROtational SPEctroscopy (PROSPE), http://info.ifpan.edu.pl/~kisiel/prospe.htm; accessed 7 February 2024.
[36]G. Wlodarczak, D. Boucher, R. Bocquet, and J. Demaison, "The microwave and submillimeter-wave spectrum of methyl chloride," J. Mol. Spectrosc. **116**(1), 251–255 (1986).
[37]A. C. Legon and J. C. Thorn, "Equilibrium nuclear quadrupole coupling constants from the rotational spectrum of BrCl: A source of the electric quadrupole moment ratios $Q(^{79}\mathrm{Br})/Q(^{81}\mathrm{Br})$ and $Q(^{35}\mathrm{Cl})/Q(^{37}\mathrm{Cl})$," Chem. Phys. Lett. **215**(6), 554–560 (1993).
[38]P. Pyykkö, "Spectroscopic nuclear quadrupole moments," Mol. Phys. **99**(19), 1617–1629 (2001).
[39]D. Sundholm and J. Olsen, "Finite element multiconfiguration Hartree–Fock determination of the nuclear quadrupole moments of chlorine, potassium, and calcium isotopes," J. Chem. Phys. **98**(9), 7152–7158 (1993).
[40]A. Javan, "Theory of a three-level maser," Phys. Rev. **107**(6), 1579–1589 (1957).
[41]T. Oka, "Observation of $\Delta J = 3$ 'forbidden' transition in ethyl iodide by the use of double resonance," J. Chem. Phys. **45**(2), 752–753 (1966).
[42]M. Fujitake and M. Hayashi, "Microwave spectrum of 1-Iodopropane: The observation of the forbidden transitions," J. Mol. Spectrosc. **127**(1), 112–124 (1988).
[43]L. Bizzocchi, C. Degli Esposti, and F. Tamassia, "Detection of perturbation-allowed $\Delta J = 2$ transitions in the millimetre-wave spectrum of $^{81}$BrNO," Chem. Phys. Lett. **293**(5–6), 441–447 (1998).
[44]C. T. Dewberry, G. S. Grubbs II, and S. A. Cooke, "A molecule with small rotational constants containing an atom with a large nuclear quadrupole moment: The microwave spectrum of *trans*-1-iodoperfluoropropane," J. Mol. Spectrosc. **257**(1), 66–73 (2009).
[45]B. E. Long, G. S. Grubbs II, J. D. Langridge, and S. A. Cooke, "Rotational spectra, nuclear quadrupole coupling tensors, and structures for $CF_3CF_2X$, X = Cl, Br," J. Mol. Struct. **1023**, 55–60 (2012).
[46]H. S. P. Müller, P. Helminger, and S. H. Young, "Millimeter and submillimeter spectroscopy of chlorine nitrate: The Cl quadrupole tensor and the harmonic force field," J. Mol. Spectrosc. **181**(2), 363–378 (1997).
[47]L. Dore, C. Puzzarini, G. Cazzoli, and A. Gambi, "Nuclear quadrupole tensors for $^{35}$Cl and $^{37}$Cl in *cis*-1-chloro-2-fluoroethylene obtained by detection of perturbation-allowed $\Delta J = 2$ and $\Delta J = 3$ transitions," J. Mol. Spectrosc. **204**(2), 262–267 (2000).
[48]D. A. Obenchain, P. Pinacho, S. Zinn, and M. Schnell, "The low-barrier methyl internal rotation in the rotational spectrum of 3-methylphenylacetylene," J. Mol. Struct. **1213**, 128109 (2020).
[49]A. Maeda, I. R. Medvedev, F. C. De Lucia, E. Herbst, and P. Groner, "The millimeter- and submillimeter-wave spectrum of $^{13}C_1$-methyl formate ($H^{13}COOCH_3$) in the ground state," Astrophys. J., Suppl. Ser. **175**(1), 138–146 (2008).
[50]J. C. Pearson, C. S. Brauer, and B. J. Drouin, "The asymmetric top–asymmetric frame internal rotation spectrum of ethyl alcohol," J. Mol. Spectrosc. **251**(1–2), 394–409 (2008).
[51]G. S. Grubbs II, W. C. Bailey, and S. A. Cooke, "Chirped pulse Fourier transform microwave spectroscopy of 1,1,2,2-tetrafluoro-3-iodopropane," Mol. Phys. **107**(21), 2221–2225 (2009).
[52]J. E. Isert, F. E. Marshall, W. C. Bailey, and G. S. Grubbs II, "Dipole forbidden, nuclear electric quadrupole allowed transitions and chirality: The broadband microwave spectrum and structure of 2-bromo-1,1,1,2-tetrafluoroethane," J. Mol. Struct. **1216**, 128277 (2020).
[53]F. E. Marshall, N. Moon, T. D. Persinger, D. J. Gillcrist, N. E. Shreve, W. C. Bailey, and G. S. Grubbs II, "High-resolution spectroscopy near the continuum limit: The microwave spectrum of *trans*-3-bromo-1,1,1,2,2-pentafluoropropane," Mol. Phys. **117**(9–12), 1351–1359 (2019).
[54]M. J. Carrillo, W. Lin, and Y. Endo, "Microwave spectrum and iodine nuclear quadrupole coupling constants of 1,1-diiodoethane," J. Mol. Spectrosc. **378**, 111419 (2021).
[55]A. R. Davies, A. G. Hanna, A. Lutas, G. A. Guirgis, and G. S. Grubbs II, "Electric dipole forbidden, quadrupole allowed transitions in the pure rotational spectrum of cyclopropylchloromethyldifluorosilane" (unpublished) (2024).
[56]J. Kraitchman, "Determination of molecular structure from microwave spectroscopic data," Am. J. Phys. **21**(1), 17–24 (1953).
[57]C. C. Costain, "Determination of molecular structures from ground state rotational constants," J. Chem. Phys. **29**(4), 864–874 (1958).
[58]L. C. Krisher and L. Pierce, "Second differences of moments of inertia in structural calculations: Application to methyl-fluorosilane molecules," J. Chem. Phys. **32**(6), 1619–1625 (1960).

[59]L. Pierce, "Note on the use of ground-state rotational constants in the determination of molecular structures," J. Mol. Spectrosc. **3**(1–6), 575–580 (1959).
[60]H. D. Rudolph, "Extending Kraitchman's equations," J. Mol. Spectrosc. **89**(2), 430–439 (1981).
[61]J. L. Duncan, D. C. McKean, P. D. Mallinson, and R. D. McCulloch, "Infrared spectra of $CHD_2Cl$ and $CHD_2CCH$ and the geometries of methyl chloride and propyne," J. Mol. Spectrosc. **46**(2), 232–239 (1973).
[62]G. A. Guirgis, D. K. Sawant, R. E. Brenner, B. S. Deodhar, N. A. Seifert, Y. Geboes, B. H. Pate, W. A. Herrebout, D. V. Hickman, and J. R. Durig, "Microwave, $r_0$ structural parameters, conformational stability, and vibrational assignment of (chloromethyl)fluorosilane," J. Phys. Chem. A **119**(47), 11532–11547 (2015).
[63]E. W. Kaiser, "Dipole moment and hyperfine parameters of $H^{35}Cl$ and $D^{35}Cl$," J. Chem. Phys. **53**(5), 1686–1703 (1970).